Fall 2009

Determination of Stability and Control Derivatives for a Modern Light Composite Twin Engine Airplane

Monica M. Londono
Embry-Riddle Aeronautical University - Daytona Beach

DETERMINATION OF STABILITY AND CONTROL DERIVATIVES FOR A MODERN LIGHT COMPOSITE TWIN ENGINE AIRPLANE

by

Monica M. Londono

A Thesis Submitted to the
Graduate Studies Office
In Partial Fulfillment of the Requirements for the
Degree of Master of Science in Aerospace Engineering

Embry-Riddle Aeronautical University
Daytona Beach, Florida
Fall 2009

DETERMINATION OF STABILITY AND CONTROL DERIVATIVES FOR A MODERN LIGHT COMPOSITE TWIN ENGINE AIRPLANE

by

Monica M. Londono

This thesis was prepared under the direction of the candidate's thesis committee chairman, Dr. Richard "Pat" Anderson, Department of Aerospace Engineering, and has been approved by the members of her thesis committee. It was submitted to the Department of Aerospace Engineering and was accepted in partial fulfillment of the requirements for the degree of Master of Science in Aerospace Engineering.

THESIS COMMITTEE:

Dr. Richard "Pat" Anderson
Chairman

Dr. Maj Mirmirani
Member

Professor Charles Eastlake
Member

Coordinator, MSAE Program

Department Chair, Aerospace Engineering — 2/25/2010 Date

Dr. James Cunningham, Associate VP for Academics — 3/10/10 Date

ACKNOWLEDGEMENTS

I would like to thank everyone who helped me and supported me in my thesis work. This project has been very important to me and its success can largely be attributed to the support I have received. I want to start by thanking my parents, brother and family. They have been a model of love, responsibility and hard work. Thank you for all the support and for always believing in me.

I would like to thank Dr. Anderson for all of his help during my time at Embry-Riddle. Thank you for everything you have taught me and for giving me the opportunity to experience so many different and exciting projects. I would also like to thank Prof. Eastlake and Dr. Mirmirani for all of their advice and knowledge which was put to good use for this thesis. I also include thanks to all the faculty and ERAU community for my growth as a person and the knowledge I have gained.

I would also like to thank my friends, classmates and all the students who supported my work. I learned a great deal from all of you and I am lucky to have such wonderful help. Dick, thank you for your help during my initial work; your programming expertise was essential. You were patient and always willing to make everything work. Brett, I thank you for our numerous discussions on everything involving flight testing that greatly clarified my understanding. Your motivation was endless and you were always willing to help; thanks for all of your support.

Thank you all for sharing this process with me which has helped me grow into the person I am today. I could not have done it without you.

ABSTRACT

Author: Monica M. Londono

Title: Determination of stability and control derivatives for a modern light composite twin engine airplane

Institution: Embry-Riddle Aeronautical University

Degree: Master of Science in Aerospace Engineering

Year: 2009

To develop and compare full envelope stability and control derivatives and their associated errors for a modern light composite twin engine airplane from flight test data and digital DATCOM (Data Compendium). This development is to serve three purposes 1) to provide data for validation of newer analytical techniques such as Computational Fluid Dynamics (CFD), 2) to provide public domain static and dynamic stability and control derivatives for a modern twin engine airplane, 3) to analyze the relationship between test design and error for both output error and equation error methods.

A flight test program was conducted on a Diamond Twin Star DA42 with Thielert engines and on a DA42 with Lycoming engines by Embry-Riddle Aeronautical University. For the theoretical verification the equation error and output error methods in both time and frequency domain within System Identification Programs for AirCraft (SIDPAC), were used. The DATCOM analysis was based on airplane drawings and direct measurement on the DA42 airframe. The results for both methods and error associated with SIDPAC were compared to Digital DATCOM results.

TABLE OF CONTENTS

TABLE OF FIGURES

LIST OF ACRONYMS

AFM	Airplane Flight Manual
AMM	Airplane Maintenance Manual
C.G.	Center of Gravity
CFD	Computational Fluid Dynamics
DA42 L360	Twin Star DA42 with Lycoming Engines
DA42 TDI	Twin Star DA42 with Thielert Engines
DATCOM	Data Compendium
EE	Equation Error
ERAU	Embry-Riddle Aeronautical University
OE	Output Error
PID	Parameter Identification
SCF	Scale factor
SIDPAC	System Identification Programs for AirCraft

NOMENCLATURE

α	Angle of attack
β	Angle of sideslip
δ_a	Aileron deflection
δ_e	Elevator deflection
δ_r	Rudder deflection
λ	Scale factor error on measured parameter
□, θ, ψ	Roll, pitch and heading Euler angles
a_x, a_y, a_z	Components of linear acceleration along the x, y, z body reference axes
b	Bias error on measured parameter
$\bar{c}$	Mean Aerodynamic Chord
CL	Lift force coefficient
Cl	Rolling moment coefficient
Cm	Pitching moment coefficient
Cn	Yawing moment coefficient
CX	Force along the x body reference axis
CY	Force along the y body reference axis
CZ	Force along the z body reference axis
g	Acceleration due to gravity
I_{xx}, I_{yy}, I_{zz}	Moment of inertias about the x, y, z body reference axes
I_{xy}, I_{xz}, I_{yz}	Products of inertia
M, L, N	Moments about the x, y, z body reference axes
m	Aircraft mass
p, q, r	Components of angular velocity about the x, y, z body reference axes
PPT	Precision Pressure Transducer
$\bar{q}$	Dynamic pressure
S	Reference wing area
T	Aircraft thrust
u, v, w	Components of linear velocity along the x, y, z body reference axes
V	True airspeed
X, Y, Z	Forces along the x, y, z body reference axes
x_{cg}	Aircraft center of gravity longitudinal location
x_{ref}	Aircraft reference center longitudinal location

Notation:

$\dot{\ }$	First derivative with respect to time
$\hat{\ }$	Non-dimensional angular rates

Subscripts used with coefficients:

α	Derivative with respect to alpha
β	Derivative with respect to beta
δ_a	Derivative with respect to ailerons

δ_e	Derivative with respect to elevator
δ_r	Derivative with respect to rudder
cg	Moment about the center of gravity
p	Derivative with respect to roll rate
q	Derivative with respect to pitch rate
r	Derivative with respect to yaw rate
ref	Moment about a reference location

1. INTRODUCTION

The proposed thesis topic is to develop and compare a full envelope stability and control derivatives and their associated errors for a modern light composite twin engine airplane from flight test data and digital DATCOM (Data Compendium). For the theoretical verification methods the MATLAB based software *System Identification Programs for AirCraft* (SIDPAC) was used. The methods used include equation error and output error in time and frequency domain. The flight test data is based on two flight test projects conducted by Embry-Riddle Aeronautical University. The first project took place on Fall 2007 and involved a DA42 with Thielert engines. In Spring of 2009, the newer version of the DA42 was tested. In this version, the Thielert engines were replaced with Lycoming engines.

For the digital DATCOM analysis the drawings and information in the airplane flight manual (AFM) and the maintenance manual (AMM) were used. In addition, some direct measurements on the airplane were done to gather information on the wing, horizontal and vertical tail airfoils. For the comparison the input file for digital DATCOM was set to match the flight conditions flown during the flight test program for the DA42TDI.

The development of this thesis is to serve three purposes 1) to provide data for validation of newer analytical techniques such as Computational Fluid Dynamics (CFD), 2) to provide public domain static and dynamic stability and control derivatives for a modern twin engine airplane, 3) to analyze the relationship between test design and error for both output error and equation error methods.

1.1 PID Background

System identification is based on the development of mathematical models that explain a system based on imperfect observations of its behavior. A widely accepted definition is the one given by Zadeh:

"System identification is the determination on the basis of observation of input and output, of a system within a specified class of systems to which a system under test is equivalent" [1]

The main objective is to create a mathematical model that represents the systems accurately. A very important application of system identification is the estimation of the stability and control derivatives for aircraft.

Usually the dynamics of an aircraft can be explained using models with known structures, making the main goal of system identification the estimation of the parameters within the model. For this reason, system identification for aircraft is commonly known as parameter identification (PID).

1.1.1 SIDPAC Background

SIDPAC is a collection of MATLAB files developed by Dr. Eugene Morelli at NASA Langley in 1992. This software has been used to analyze flight test, wind-tunnel and simulation data. Some of the functions included in SIDPAC involve algorithms for data compatibility, model structure determination, and parameter identification methods on both time and frequency domain.

1.1.2 Digital DATCOM Background

Digital DATCOM is a computer program based on the USAF Stability and Control DATCOM. This program calculates airplane stability and control derivatives at different flight conditions. To estimate the derivatives digital DATCOM requires the user to input a flight condition and geometric characteristics of the aircraft.

1.2 Airplane Information

The following are general characteristics of the Twin Star DA42 airplane:

- Mean Aerodynamic chord: 4.167 ft
- Wing Span: 44ft
- Wing Area: 175.3 ft^2
- Aspect Ratio: 11.06
- Empty Weight: 2,804 lbs
- Max. Take-off Weight: 3,935 lbs
- Airframe : Carbon Composite

The aircraft used for the DA42TDI flight test program was:

Airframe:

- Manufacturer: Diamond Aircraft Industries GmbH
- Model: Twin Star DA-42, A57CE
- Serial Number: 42.213

Engines:

- Manufacturer: Thielert
- Model: TAE 125-01, E00069EN
- Left Serial Number: 02-01-1082

- Right Serial Number: 02-01-1084

Propellers:

- Manufacturer: MT Propeller Co.
- Model: MTV-6-A-C-F/CF187-129, P19NE
- Left Serial Number: 06925
- Right Serial Number: 06926

The aircraft used for the DA42L360 flight test program was:

Airframe:

- Manufacturer: Diamond Aircraft Industries GmbH
- Model: Twin Star DA-42L360
- Serial Number: 42.AC132

Engines:

- Manufacturer: Lycoming Engines
- Model: Lycoming L/IO-360-M1A

Propellers:

- Manufacturer: MT Propeller Co.
- Model: MTV-12-B-C-F/CF(L)183-59b

1.3 Sign Convention

The figure below illustrates the sign convention used in the flight test program and in this study. It is such that positive surface deflections yield negative aerodynamic moments. All the flight test measurements are in a body axis.

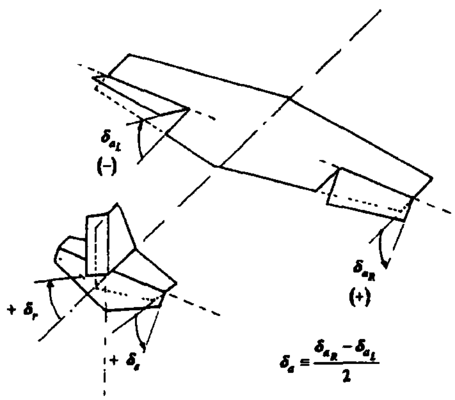

Figure 1 Control Surface Sign Convention

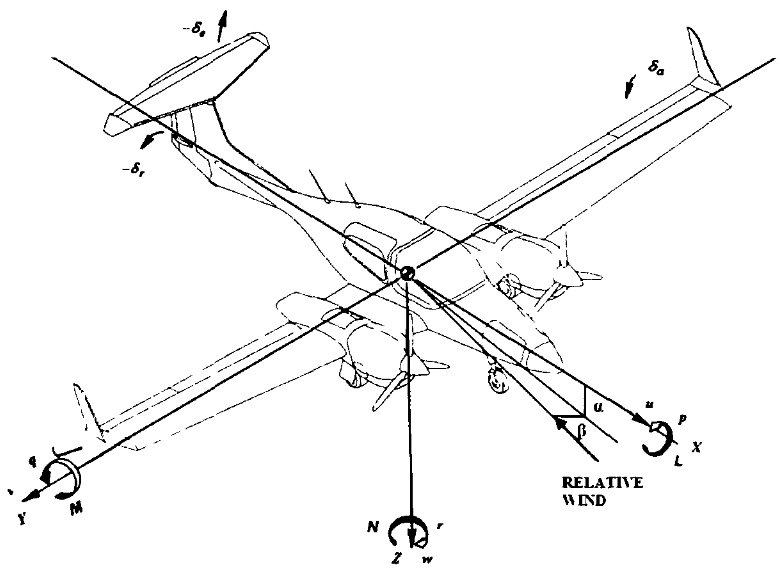

Figure 2 Airplane Notation and Sign Convention

1.4 Literature Review

1.4.1 PID methods

A wide variety of PID methods exist. Three of the most common are: equation error, output error and filter error. The main differences between these methods are the assumptions that simplify each of them. The filter error is the most general but it is rarely use in practice due to its complexity. Equation error and output error are widely used in the aerospace industry.

1.4.2 Equation error

Equation error is known for its simplicity, it uses the least squares method to minimize the error in a given equation. It is also known as linear regression analysis, since it is modeling the relationship between the measured variables.

The first step when using this method is to determine the model or equation. The following example shows a possible model for the pitching moment coefficient.

$$Cm = Cm_{\alpha}a + Cm_{\hat{q}}\hat{q} + Cm_{\delta e}\delta e + Cm_o + v \qquad (1)$$

In this equation Cm is the dependent variable, also called the output; α, q and δe are the independent variables, also called regressors. The variable Cm_o is the model bias of the dependent variable, and it usually represents the trim value. The random error in the equation is represented by the variable v. Finally, Cm_{α}, Cm_q and $Cm_{\delta e}$ are the parameters of the model, also known as the stability and control derivatives for the pitching moment coefficient. The objective of the PID analysis is to find estimates for those parameters. It is important to notice the output is linear with respect to the parameters.

The equation error method calculates values for the parameters by minimizing the cost function of the equation and the results can be obtained by applying matrix algebra operations in a one step computational procedure[2]. This method is very practical because it finds an estimate for the parameters without need for iterations.

The simplicity of this method is due to several important assumptions. It is very important when analyzing data to take into account these assumptions since they can affect the results. The main assumptions are:

- All states and state derivatives are measured directly
- The independent variables are measured without error
- The dependent variable is measured with uniformly distributed noise
- The residuals are assumed to be white

To account for the last two assumptions the error can be corrected for colored residuals. In reality the errors on the independent variables are never zero. This is one of the biggest disadvantages of this method. The error within the independent variables can yield biased estimation of the parameters[2]. To counteract this assumption the data can be pre-processed before applying the equation error technique. Some of the pre-processing involves smoothing the data and kinematic compatibility analysis.

In addition, from equation (1) it is noticed that the data points required to obtain an answer will depend on the number of regressors if v is assumed to be zero. However, on practical problems v is never zero requiring more data points. As a result, it becomes an over-determined problem to average out the noise effects on the parameter estimation. More data points are beneficial to average out the noise which improves parameter estimation results[2].

This method is characterized by its simplicity and the possibility of analyzing each force and moment coefficient individually. These facts make the equation error method very useful in the model structure determination and to obtain initial estimates for the derivatives.

1.4.3 Output error

The output error is a maximum likelihood estimation method with some restrictions. The output error parameter estimation is done by minimizing the weighted sum squared errors for several outputs at once[2], becoming an iterative process. Some of the assumptions for the output error method are:

- There is no process noise in the equations
- The control variables are measured without error
- The residuals are uncorrelated

The first assumption is usually not a critical one. Process noise generally accounts for atmospheric turbulence, pilot neuromuscular noise and control input noise[3]. Almost all flight test programs try to minimize process noise by flight testing in a very calm atmosphere.

The output error method usually uses the equations of motion so that the lateral or longitudinal model parameters are estimated together. The following example illustrates a case for a longitudinal PID analysis:

$$\dot{\alpha} = \frac{\dot{w} \cdot u - \dot{u} \cdot w}{(u^2 + w^2)} + bias_{\dot{\alpha}} \qquad (2)$$

$$\dot{\theta} = q\cos(\phi) - r\sin(\phi) + bias_{\dot{\theta}} \qquad (3)$$

$$\dot{q} = \left(\left(\frac{I_{zz} + I_{xx}}{I_{yy}}\right) \cdot p + \left(\frac{1}{I_{yy}}\right) I_{\mathrm{p}}\Omega_{\mathrm{p}}\right) \cdot r + \left(\frac{I_{xz}}{I_{yy}}\right)(r^2 - p^2) + \bar{q} \cdot S \cdot \bar{c}\left(\frac{1}{I_{yy}}\right) C_m + bias_q$$

$$a_z = \frac{\bar{q} \cdot S \cdot CZ}{m} + bias_{a_z} \qquad (5)$$

Where,

$$\dot{u} = rv - qw + \frac{\bar{q}S}{m} CX + g \cdot sin(\theta) + \frac{T}{m} \qquad (6)$$

$$\dot{w} = qu - pv + \frac{\bar{q}S}{m} CZ + g \cdot cos(\theta) \sin(\phi) \qquad (7)$$

$$CX = \frac{ma_z - T}{\bar{q}S} \qquad (8)$$

$$Cm = Cm_{\alpha}a + Cm_{\hat{q}}\hat{q} + Cm_{\delta e}\delta e \qquad (9)$$

$$CZ = CZ_{\alpha}a + CZ_{\hat{q}}\hat{q} + CZ_{\delta e}\delta e \qquad (10)$$

The state equations (2), (3) and (4) are integrated and the solution for the parameter is found by an iterative nonlinear optimization. As a consequence, the output error can be used in nonlinear problems.

The iterative nature of the output error process can encounter some problems that might result in the method diverging, without being able to find a solution for the parameters. Some of these problems could be caused by:

- Having too many parameters and data with not enough useful content. This problem is known as over-parameterization.
- Having two or more parameters-regressors that cause almost the same effects on the model. This problem can be avoided by checking the collinearity between the regressors before applying the PID method.
- Not having enough movement on the outputs

The output method is a very powerful method that has been used in many different programs in the aerospace industry. For final results, engineers usually prefer to use the output error method over the equation error method since it produces more accurate results.

1.4.4 Data compatibility

For parameter identification the quality of the data measured is critical in order to create an accurate mathematical model that describes the system. The data required for the parameter identification process depends on the method used and the application. Some of the most common required parameters for aircraft PID are:

- Time
- True airspeed (speed, temperature, pressure altitude)
- Density (temperature, pressure altitude)
- Flow angles: alpha and beta
- Angular rates: p, q, r
- Mass properties: cg, weight, moments of inertia
- Body accelerations: a_x, a_y, a_z
- Thrust
- Euler angles: □, θ, ψ
- Control surfaces: δe, δa, δr

Some common errors found on the measurements are scale factors, biases and time lags. There are different ways in which those errors can be found with the objective of improving the measurements. One common procedure to achieve this is to run a data compatibility check before the PID process.

1.4.4.1 Flight path reconstruction

The flight path reconstruction method uses the aircraft kinematic equations of motion to check data computability. It can be used to find scale factors, biases and time lags on the data. In the following discussion the focus will be the estimation of scale factors and biases.

The kinematic equations can be used with the output error methods to estimate the biases and scale factors on the measurements. This is done the by setting the biases and scale factors as the unknown parameters on the output error algorithm. Generally the longitudinal motion and the lateral-directional motion data compatibility checks are done separately. This is because it is not common to have maneuvers with enough excitation on all three axes. The following set of equations is for a longitudinal data compatibility analysis[1]:

$$\dot{u} = (r - b_r)v - (q - b_q)w - gsin(\theta) + a_x - b_{ax}$$

$$\dot{w} = (q - b_q)u - (p - b_p)v + gcos(\theta)\cos(\phi) + a_y - b_{ay}$$

$$\dot{\theta} = \cos(\phi)\,(q - b_q) - \sin(\phi)\,(r - b_r)$$

Outputs,

$$V = (1 - \lambda_V)\left(\sqrt{u^2 + v^2 + w^2} + V_o\right) + b_V + V_o + v_V$$

$$\alpha = (1 - \lambda_\alpha)\left(tan^{-1}\left(\frac{w}{u}\right) + \alpha_o\right) + b_\alpha + \alpha_o + v_\alpha$$

$$\theta = (1 - \lambda_\theta)\theta + b_\theta + v_\theta$$

The speed and angle of attack equations are written in a way to try to minimize the correlation between the scale factors and the biases. On the example above, the angular rates (p, q, r) and the linear accelerations (ax, ay, az) are the inputs to the system. The angle of attack (α), speed (V), and theta (θ) are the outputs.

Unfortunately, there is no way of checking the control surface measurements; for this reason, special attention should be paid during the calibration of these signals.

2. METHODS

2.1 PID analysis

The following flowchart describes the process that was used to analyze the flight test data collected for the DA42TDI and the DA42L360 programs. The methods used to analyze the data were equation error and output error methods in time and frequency domain. In the following sections, specific steps of this flowchart are described in detail.

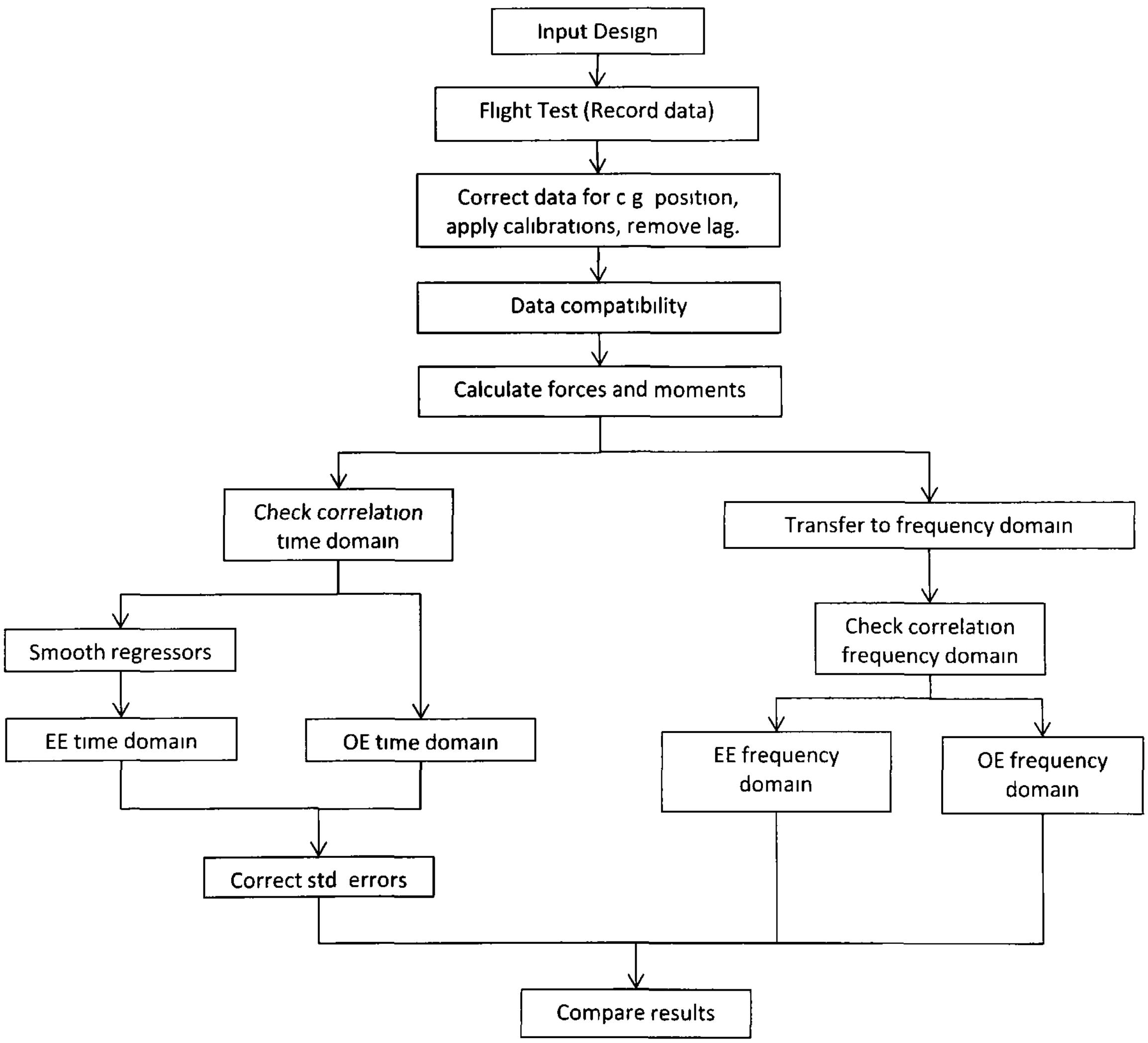

Figure 3 PID Analyses Flowchart

2.2 Test Input Design

There are specific flight test maneuvers that are used for PID analysis. Some of these maneuvers include the following control inputs:

- Pulses
- Steps
- Multistep
    - Doublets
    - 3-2-1-1
- Frequency sweeps
- Multi-sines

In general the main goal of these inputs is to excite the different dynamic modes of the aircraft. Some of the considerations for the input design are to produce maneuvers with:

- Enough data information (proper mode excitation and high signal-to-noise ratio)
- Low correlation between parameters
- Small perturbations around the trim point to remain in the linear region
- Practical constraints

Low correlation between the parameter is a key factor of the input design process. In general, high correlation is an indication of data collinearity. For PID analysis a correlation factor of 0.9 or higher between the regressors usually will result in poor parameter estimation[1]. Independent control inputs are performed to avoid high correlation between the control surfaces.

2.2.1 Longitudinal Inputs

The excitation of the short period is usually used to estimate the longitudinal stability and control derivatives. The short period can be excited with an elevator input or other longitudinal control. Doublets and 3-2-1-1 are usually used as elevator inputs to excite the short period. Sometimes, the 3-2-1-1 is preferable for flight test data over the doublet since it has a wider frequency band. The wider frequency band is desirable since the exact frequency of the short period is unknown.

During the DA42TDI and the DA42L360 the longitudinal PID maneuver consisted of 3-2-1-1 at different speeds and angle of attacks. The following figure shows the elevator deflection for a 3-2-1-1 pilot input in the DA42TDI flight test program.

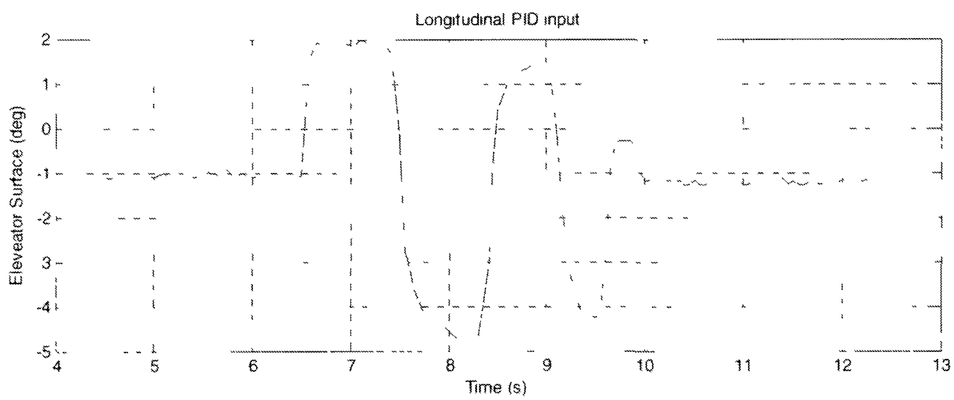

Figure 4 DA42TDI/DA42L360 Longitudinal PID Input

The short period excitation is desirable for some longitudinal PID analysis since there is low correlation between angle of attack and pitch rate. In the following figure the time histories of these regressors can be compared during a 3-2-1-1 maneuver.

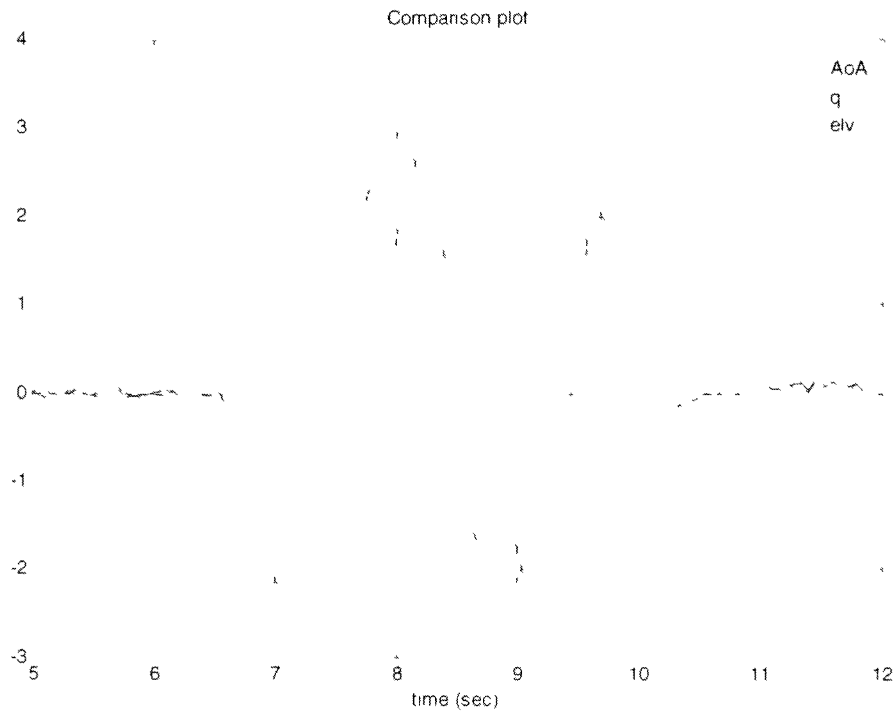

Figure 5 Longitudinal regressors during 3-2-1-1 maneuver

2.2.2 Lateral-directional Inputs

Because of the coupling between the lateral directional motions the stability and control derivatives for these modes are usually estimated together. To evaluate the lateral mode a bank–to-bank maneuver or aileron doublet can be used. For the directional mode it is desired to estimate the dutch-roll. The dutch-roll is a lightly damped mode and generally any input will be enough to excite it; rudder doublets are commonly used. It is recommended to do the lateral and directional inputs in the same maneuver to minimize the correlations between the regressors.

On the DA42TDI flight test program the lateral-directional PID maneuver consisted of rudder doublet follow by an aileron doublet. In most cases, the pilot waited at least one oscillation of the dutch-roll before executing the aileron doublet. It was decided to do the rudder input first since it is a slower mode than the roll-mode.

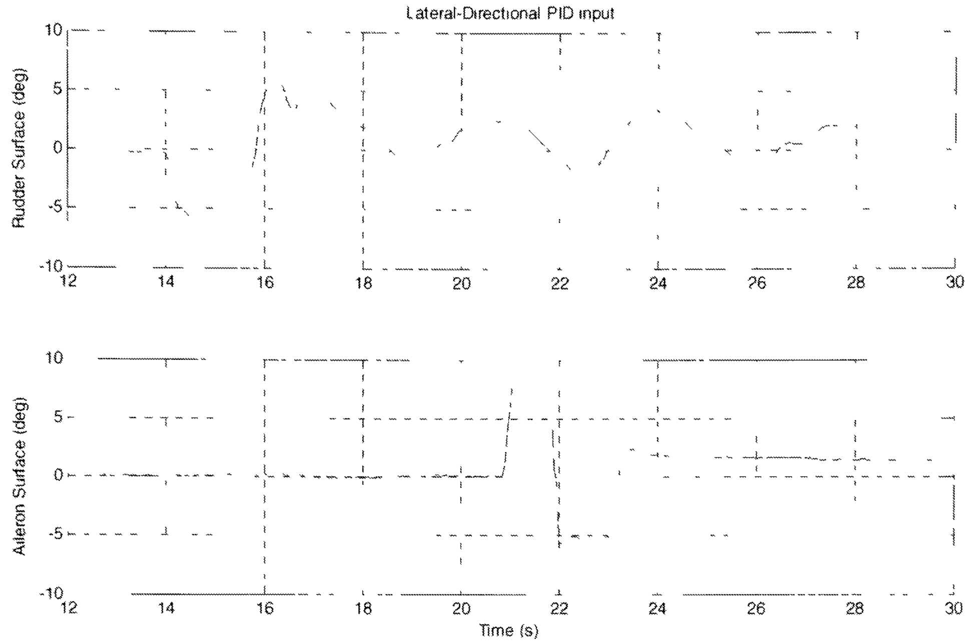

Figure 6 DA42TDI Lateral-Direction PID input

On the DA42L360 test program the lateral-directional input was modified by making the aileron input longer. The aileron was held until a bank angle of 30 degrees was achieved, then opposite aileron was held until bank angle reached the opposite 30 degree point. The intention of this modification on the lateral-directional input was to make the aileron deflection longer in order to try to capture a yawing moment derivative due to the ailerons (Cn_{da}). However, estimation of the Cn_{da} is not included on the scope of this research project.

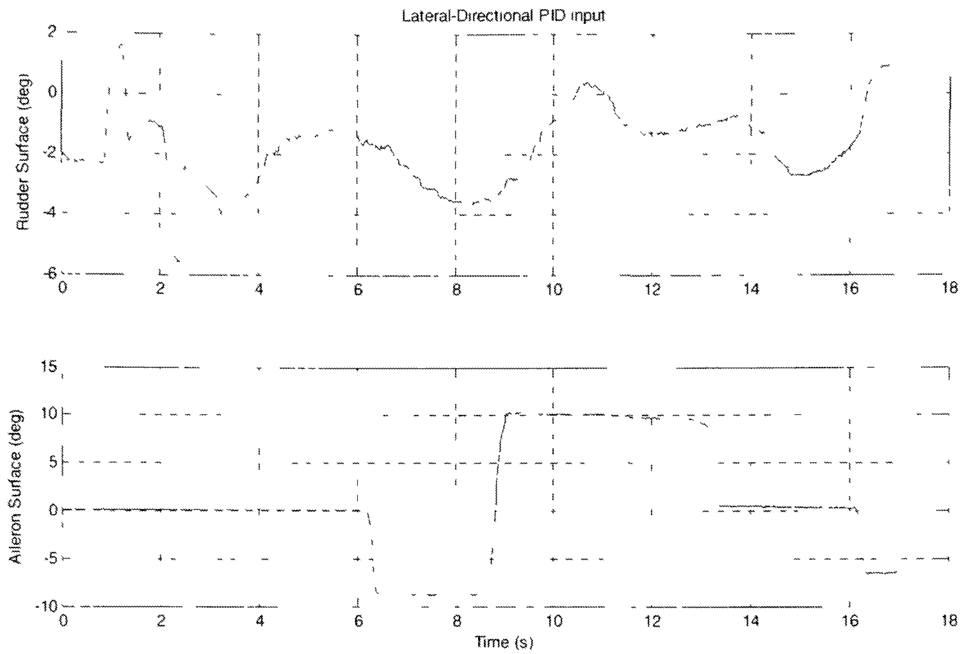

Figure 7 DA42L360 Lateral-Directional PID Input

2.3 Flight test data and Instrumentation

2.3.1 Instrumentation

The following table is a list of the main raw parameters recorded during each flight test program and used in this study. The rate for data collection on the DA42TDI was 20 Hz and the rate for the DA42L360 was 50 Hz.

Table 1 Flight Test Raw Parameters

Variable	Instrument	Accuracy
Time	SPAN GPS/IMU INS	20 ns
IAS	Honeywell Precision Pressure Transducer (PPT)	0.01 psi
OAT	G1000/Thielert engine	1 degree C
Altitude (h)	Honeywell PPT	0.01 psi
Alpha (α)	Vane/Potentiometer	--
Beta (β)	Vane/Potentiometer	--
Roll rate (p)	SPAN GPS/IMU INS	--
Pitch rate (q)	SPAN GPS/IMU INS	--
Yaw rate (r)	SPAN GPS/IMU INS	--
Roll angle (□)	SPAN GPS/IMU INS	0.015 deg
Pitch angle (θ)	SPAN GPS/IMU INS	0.015 deg
Yaw angle (ψ)	SPAN GPS/IMU INS	0.05 deg
Longitudinal acceleration (a_x)	SPAN GPS/IMU INS	0.003g
Lateral acceleration (a_y)	SPAN GPS/IMU INS	0.003g
Normal acceleration (a_x)	SPAN GPS/IMU INS	0.003g
Elevator Surface	String Pot	--
Ailerons surface	String Pot	--
Rudder surface	String Pot	--
RPM	Thielert engine instrumentation	10 RPM
Percent load output to the shaft (% Load)	Thielert engine instrumentation	Percent
Fuel Flow	Thielert engine instrumentation	0.1 GPH
Fuel Used	Thielert engine instrumentation (Calculated)	0.1 Gallon

2.3.2 Derived Parameters

In order to reconstruct forces and moment coefficients it was necessary to derive other parameters that could not be measured directly. The following is a list of the main derived parameters.

Table 2 Flight Test Derived Parameters

Derived Parameter	Required Variables	Description
True airspeed (V)	IAS, OAT, alt	True airspeed corrected for position error and density altitude
Rho (ρ)	OAT, atl	Calculated from pressure altitude at the boom and OAT
Dynamic pressure (qbar)	rho, V	Dynamic pressure calculated using the density and true airspeed parameters
Propeller Efficiency (η)	% Load, RPM, rho, V	Computed using engine parameters and MT-propeller model
Thrust	% Load, RPM, rho, V, η	Computed using the % power reported by the engine and propeller efficiency
pdot	p,T	Smoothed time derivative of roll rate
qdot	q, T	Smoothed time derivative of pitch rate
rdot	r, T	Smoothed time derivative of yaw rate

2.3.3 Mass Properties

To calculate the mass properties the airplane was weighted before and after each flight. To calculate the current weight, the fuel used was subtracted from the initial weight. To estimate the C.G. a linear interpolation between the initial and final C.G. was used as a function of weight. Also, to estimate the moments of inertia a linear interpolation between the gross moments of inertia and the empty moments of inertia was used as a function of weight. The gross and empty moments of inertia were calculated using the moments of inertia equations provided in reference 4.

2.3.4 Test Points

During each flight test program different flight conditions were flown. The flight conditions vary in airspeed, angle of attack and altitude. The following table describes the flight conditions on the DA42TDI project.

Table 3 DA42TDI Test Conditions

Flight Condition	Airspeed (knots)	Angle of Attack (deg)	Altitude (ft)
1	100	5.12	5664
2	99	4.89	5717
3	107	4.25	5675
4	103	4.00	5679
5	108	3.19	5690
6	118	1.93	5679
7	130	1.57	5664
8	139	0.84	5635
9	152	0.17	5617
10	168	0.00	5597
11	161	-0.05	5603

The following table describes the flight conditions on the DA42L360 project.

Table 4 Test Conditions

Flight Condition	Airspeed (knots)	Angle of Attack (deg)	Altitude (ft)
1	85	8.89	3687
2	91	7.20	3899
3	93	6.13	4070
4	95	6.01	4098
5	97	5.69	4151
6	103	4.52	4438
7	109	3.59	4709
8	114	2.93	4906
9	119	2.46	5013
10	124	1.67	5085
11	129	1.56	5720
12	130	1.43	5232
13	139	1.07	5805
14	141	0.67	5970
15	154	0.55	6265
16	145	0.50	6085
17	151	0.43	5137
18	147	0.37	5324
19	162	-0.02	6288

2.4 Flight Test Data Corrections

The following flowchart shows the standard flight test corrections that were applied to the flight test data.

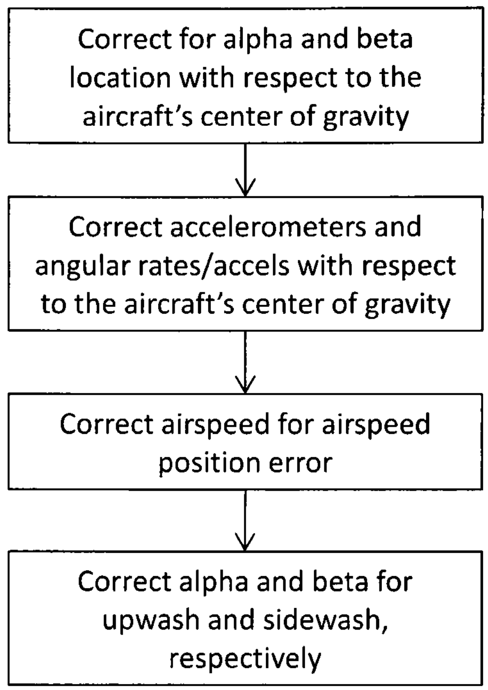

Figure 8 Flight Test Data Corrections Flowchart

2.4.1 Flight test Data Calibrations

Most of the instrumentation like the string pots and the alpha and beta vanes required calibrations. The following is an example of the calibration of the string pot used to measure the elevator surface deflection on the DA42TDI project.

The string pot was mounted on the elevator surface as it can be observed in the following picture.

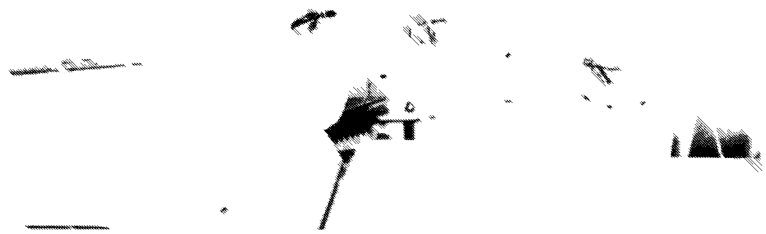

Figure 9 Elevator String Pot

To calibrate the string pot a digital inclinometer was used. With the digital inclinometer the elevator deflection was measured in degrees The calibration was done up and down of the datum. The datum was found by matching the maximum and minimum surface deflections from the type certificate data sheet for the DA42

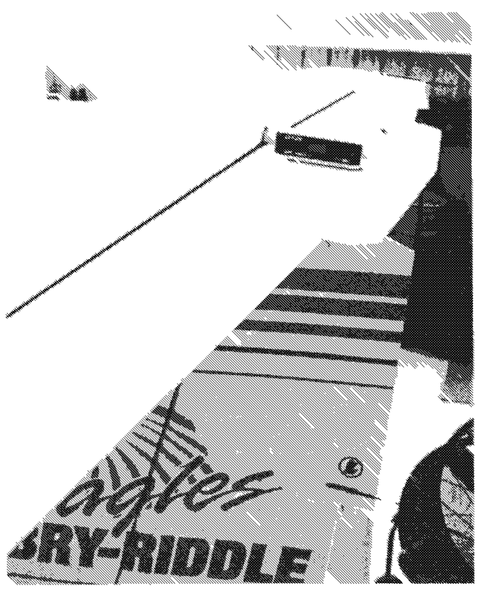

Figure 10 Elevator Calibration

The elevator deflection in degrees from the digital inclinometer was plotted vs. the voltage ratio readings of the string pot to find the relationship between the two readings. The calibration equation was approximated with a second order polynomial.

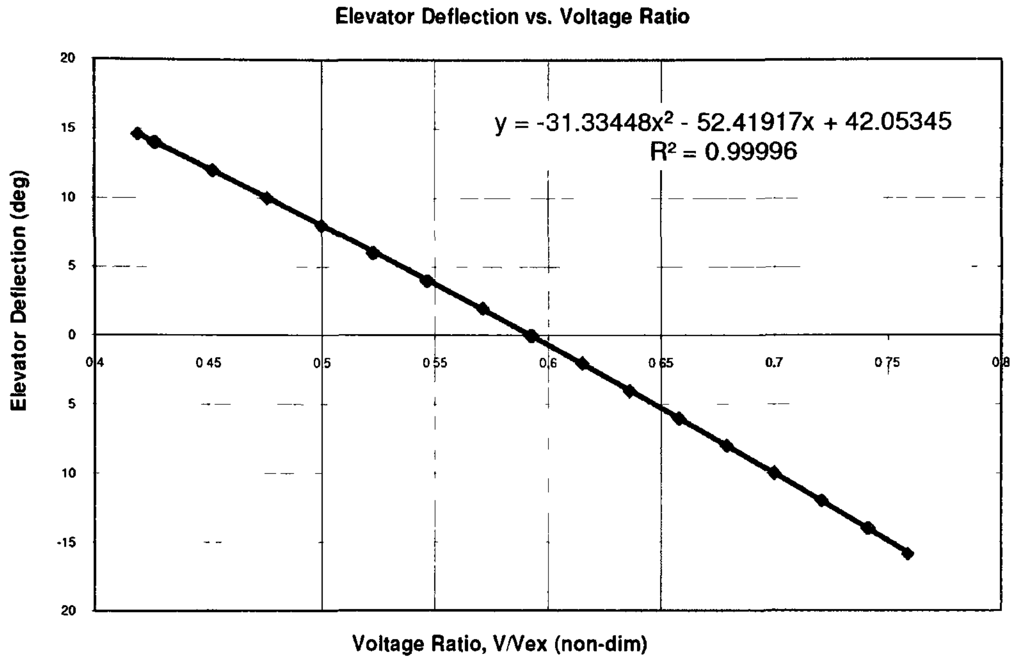

Figure 11 Elevator Deflection Angle vs. Voltage Ratio

2.5 Data Compatibility Results

Longitudinal and lateral-directional data compatibility (DCMP) analysis was run for each individual case. The data compatibility analysis was done for the longitudinal and the lateral-directional separately. The reason for this was that during the longitudinal maneuvers there was not enough excitation on the lateral- directional parameters to find associated errors, and vice versa.

The following table summarizes the errors found from all the longitudinal PID maneuvers analyzed for the DA42TDI project.

Table 5 DA42TDI Longitudinal DCMP Results

FC	ax bias (fps)	+/- ax bias	az bias (fps)	+/- az bias	q bias (dps)	+/- q bias	AoA scale factor	+/- AoA scale factor	theta scale factor	+/- theta scale factor
1	0.25	0.02	-0.04	0.03	0.00	0.00	-0.12	0.01	0.00	0.00
2	0.31	0.03	-0.15	0.02	-0.05	0.00	-0.15	0.01	0.01	0.00
3	-0.01	0.01	-0.06	0.01	0.00	0.00	-0.10	0.01	-0.01	0.01
4	-0.08	0.01	0.00	0.04	-0.11	0.01	-0.24	0.03	-0.07	0.01
5	0.12	0.01	0.27	0.06	0.06	0.01	-0.16	0.03	0.03	0.01
6	0.03	0.01	0.13	0.04	0.05	0.00	-0.18	0.02	0.04	0.01
7	-0.04	0.01	0.16	0.04	-0.08	0.01	-0.21	0.02	-0.04	0.01
8	-0.13	0.01	0.03	0.05	0.13	0.01	-0.12	0.03	-0.04	0.01
9	0.04	0.01	0.18	0.05	0.01	0.00	-0.12	0.02	0.01	0.01
10	-0.20	0.01	-0.05	0.08	-0.13	0.01	-0.19	0.04	-0.09	0.01
11	-0.09	0.01	-0.03	0.07	-0.05	0.01	-0.15	0.03	-0.04	0.01

The DA42TDI longitudinal DCMP model was also applied on the DA42L360 data. The results are summarized on the following table.

Table 6 DA42L360 Longitudinal DCMP Results

FC	ax bias (fps)	+/- ax bias	az bias (fps)	+/- az bias	q bias (dps)	+/- q bias	AoA scale factor	+/- AoA scale factor	theta scale factor	+/- theta scale factor
1	1.63	0.01	0.52	0.02	0.00	0.00	0.02	0.01	0.00	0.00
2	2.16	0.01	0.14	0.01	0.01	0.00	0.01	0.01	0.00	0.00
3	1.81	0.01	0.43	0.02	-0.01	0.00	0.04	0.01	0.00	0.00
4	2.08	0.01	0.15	0.02	0.02	0.00	0.09	0.01	0.00	0.00
5	1.87	0.01	0.17	0.02	0.02	0.00	0.10	0.01	0.00	0.00
6	1.79	0.01	0.01	0.02	0.01	0.00	0.04	0.01	0.00	0.00
7	1.66	0.01	0.48	0.02	0.00	0.00	0.06	0.01	0.00	0.00
8	1.78	0.02	0.21	0.03	0.03	0.00	0.05	0.01	0.00	0.00
9	1.70	0.01	-0.03	0.02	-0.04	0.00	0.06	0.01	0.01	0.00
10	1.31	0.02	-0.03	0.03	-0.02	0.00	0.05	0.01	0.01	0.00
11	1.55	0.01	-0.41	0.03	-0.01	0.00	0.03	0.01	0.00	0.00
12	1.69	0.01	0.24	0.02	0.02	0.00	0.00	0.01	0.00	0.00
13	1.53	0.02	0.19	0.02	0.01	0.00	0.04	0.01	0.01	0.00
14	1.80	0.01	0.07	0.02	0.04	0.00	0.01	0.01	0.01	0.00
15	2.03	0.01	-0.35	0.03	0.02	0.00	0.01	0.01	-0.01	0.00
16	1.25	0.02	0.32	0.03	-0.02	0.00	0.01	0.01	0.00	0.00
18	1.66	0.01	-0.12	0.01	-0.09	0.00	0.02	0.01	0.00	0.00
19	2.21	0.02	-0.66	0.03	0.00	0.00	0.00	0.01	0.00	0.00

The results from the lateral-directional DCMP analysis for the DA42TDI are summarized on the following table.

Table 7 DA42TDI Lateral-Directional DCMP Results

FC	ay bias (fps)	+/- ay bias	p bias (dps)	+/- p bias	r bias (dps)	+/- r bias	beta scf	+/- beta bias (rad)	phi scf	+/- phi scf	psi scf	+/- phi scf
1	0.02	0.01	0.02	0.00	0.02	0.00	-0.09	0.01	0.00	0.00	0.02	0.00
3	0.04	0.02	-0.03	0.00	0.01	0.00	-0.04	0.01	0.00	0.00	0.00	0.00
4	0.02	0.01	0.01	0.00	0.00	0.00	-0.10	0.00	0.00	0.00	-0.01	0.00
5	0.01	0.01	0.04	0.00	0.00	0.00	-0.07	0.01	0.00	0.00	0.00	0.00
6	-0.12	0.01	0.01	0.00	-0.02	0.00	-0.07	0.01	0.01	0.00	-0.01	0.00
7	-0.01	0.02	-0.03	0.00	0.02	0.00	-0.09	0.01	-0.02	0.00	0.01	0.00
8	-0.12	0.02	-0.02	0.00	-0.03	0.00	-0.08	0.01	-0.01	0.00	-0.01	0.00
9	-0.09	0.02	-0.01	0.00	0.00	0.00	-0.06	0.01	-0.01	0.00	0.00	0.00
10	0.04	0.02	-0.01	0.00	0.01	0.00	-0.07	0.01	-0.01	0.00	0.00	0.00
11	-0.13	0.02	-0.01	0.00	-0.01	0.00	-0.07	0.01	-0.01	0.00	0.00	0.00

The DA42TDI lateral-directional DCMP model was also applied on the DA42L360 data. The results are summarized on the following table.

Table 8 DA42L360 Lateral-Directional DCMP Results

FC	ay bias (fps)	+/- ay bias	p bias (dps)	+/- p bias	r bias (dps)	+/- r bias	beta scf	+/- beta scf	phi scf	+/- phi scf	psi scf	+/- phi scf
1	-0.12	0.01	0.01	0.00	0.00	0.00	-0.03	0.00	-0.02	0.00	0.00	0.00
2	-0.30	0.01	0.02	0.00	0.00	0.00	-0.08	0.01	-0.03	0.00	0.00	0.00
3	-0.62	0.01	0.08	0.00	0.01	0.00	-0.04	0.00	0.00	0.00	0.00	0.00
4	0.66	0.01	-0.08	0.00	0.01	0.00	-0.05	0.00	0.02	0.00	-0.01	0.00
5	-0.33	0.01	0.06	0.00	0.02	0.00	0.06	0.00	0.00	0.00	0.00	0.00
6	0.10	0.01	0.03	0.00	-0.01	0.00	-0.05	0.01	-0.01	0.00	0.00	0.00
7	-0.25	0.01	0.05	0.00	-0.01	0.00	-0.04	0.00	0.00	0.00	0.00	0.00
8	-0.01	0.01	0.03	0.00	0.00	0.00	-0.11	0.01	0.00	0.00	0.00	0.00
10	-0.26	0.01	0.02	0.00	0.02	0.00	-0.17	0.01	0.00	0.00	0.00	0.00
11	0.34	0.01	0.05	0.00	0.00	0.00	-0.19	0.01	0.00	0.00	0.00	0.00
13	-0.15	0.01	0.03	0.00	0.01	0.00	-0.22	0.01	0.00	0.00	0.00	0.00
14	0.10	0.01	0.06	0.00	-0.01	0.00	-0.10	0.01	0.00	0.00	0.01	0.00
16	-0.42	0.01	0.02	0.00	0.00	0.00	-0.17	0.01	0.01	0.00	0.00	0.00
15	0.54	0.02	0.00	0.00	0.01	0.00	-0.17	0.01	0.00	0.00	0.00	0.00
17	0.72	0.02	0.00	0.00	0.01	0.00	-0.22	0.01	0.00	0.00	0.00	0.00
18	0.81	0.01	0.02	0.00	0.00	0.00	-0.21	0.01	0.00	0.00	0.01	0.00
19	0.55	0.02	0.03	0.00	0.00	0.00	-0.23	0.01	0.00	0.00	-0.01	0.00

The biases on the accelerations were expected to be relatively constant for all the cases, which disagrees with what was found. A possible explanation for this is that the errors related to the INS parameters are so small that they are not being calculated accurately. However, the biases for the accelerometers were still included on the data compatibility model to prevent any random walk on the reconstruction of alpha and beta. The following graph shows the reconstruction of speed, alpha and theta without any corrections applied. In this graph it can be observed that there is almost no random walk in alpha which indicates very small biases in the accelerations.

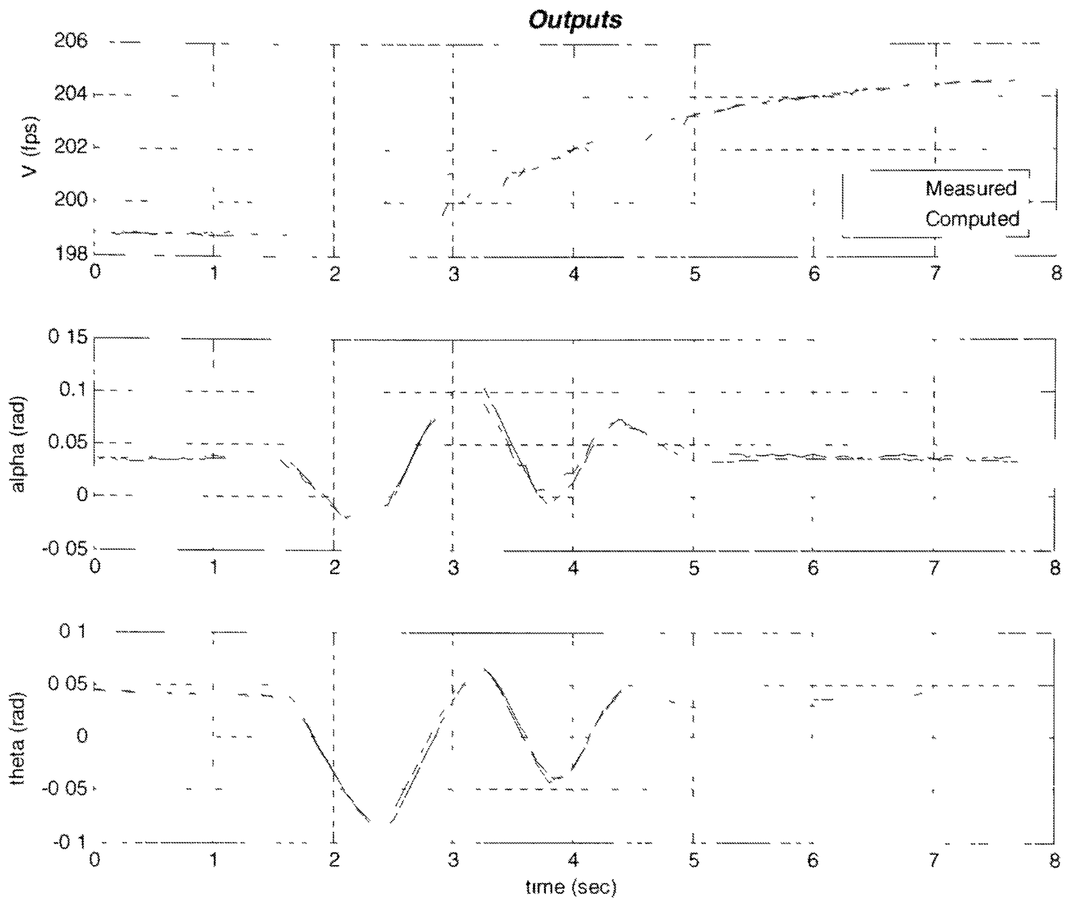

Figure 12 Longitudinal parameter reconstruction before DCMP corrections

The most significant errors found on the data were a scale factors on the angle of attack and side slip angle measurement. Usually the scale factor on alpha and beta is created by local flow fields at the sensor. The scale factor on alpha and beta are very critical since if not corrected that error will transfer directly into the alpha and beta stability derivatives. The scale factor also depends on the instrumentation and calibration equations applied to alpha and beta. Different calibrations were performed for each flight test program. The following plot shows the scale factor for alpha.

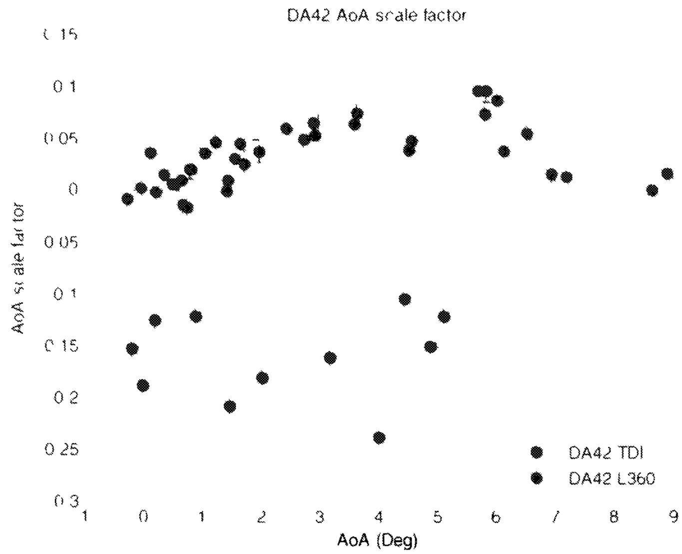

Figure 13 AoA scale factor from Longitudinal DCMP

The following plot shows the scale factor for beta.

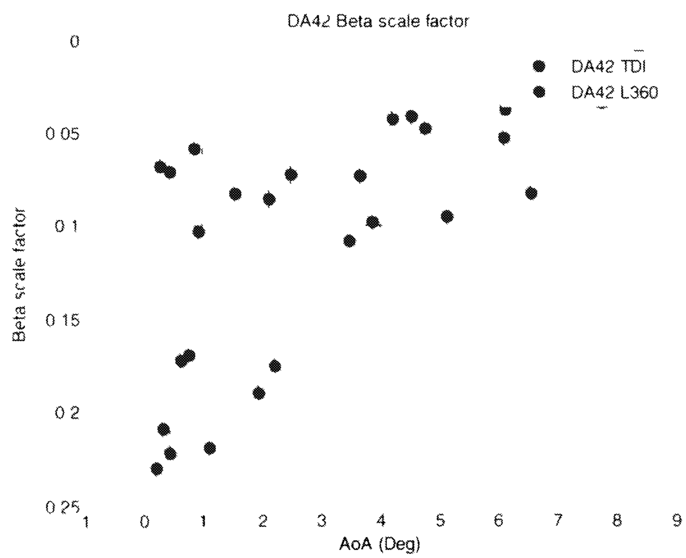

Figure 14 Beta scale factor from Lateral-Directional DCMP

2.6 Modification to SIDPAC model

It was desired to estimate the stability and control derivatives in a wind axis. Usually, PID analysis is preferable in a body axis since there is less error in the estimation of the force and moment coefficients. This is due to the fact that to be transformed into the wind axis they have to be multiplied by alpha and beta. Alpha and beta measurements inherently contain error and using them for coordinate transformations introduces that error into other parameters.

The aerodynamic models provided by SIDPAC were modified to change the forces from a body axis to a wind axis. The following equations represent the used model.

$$CX = \frac{ma_x}{\bar{q}S}$$

$$CL = CL_\alpha \alpha + CL_q q + CL_{\delta e}\delta e + CL_o$$

$$CZ = \frac{CX \cdot \sin(\alpha) - CL}{\cos(\beta)}$$

It was also desirable to calculate the pitching moment derivatives about at a reference point instead of at the c.g. position. The following equations represent the used model:

$$Cm_{ref} = \frac{1}{\bar{q}Sc}\left[I_y\dot{q} + (I_x - I_z)pr + I_{xz}(p^2 - r^2)\right]$$

$$Cm_{ref} = Cm_{cg} - \frac{(x_{cg} - x_{ref})}{\bar{c}}CZ$$

$$Cm_{ref} = Cm_\alpha \alpha + Cm_q q + Cm_{\delta e}\delta e + Cm_o$$

2.7 Linear Models

The linear models used on the DA42 PID analysis were chosen using a stepwise regression method. The stepwise method can be use to see the correlation between the parameters and other statistical numbers of a specific model. For an example of a stepwise regression refer to appendix A.

The following are the models used in the longitudinal analysis:

$$CL = CL_{\alpha}a + CL_0$$

$$Cm = Cm_{\alpha}a + Cm_{\hat{q}}\hat{q} + Cm_{\delta e}\delta e + Cm_0$$

The following are the models used in the lateral-directional analysis:

$$CY = CY_{\beta}\beta + CY_0$$

$$Cl = Cl_{\beta}\beta + Cl_{\hat{p}}\hat{p} + Cl_{\hat{r}}\hat{r} + Cl_{\delta a}\delta a + Cl_0$$

$$Cn = Cn_{\beta}\beta + Cn_{\hat{p}}\hat{p} + Cn_{\hat{r}}\hat{r} + Cn_{\delta r}\delta r + Cn_0$$

2.8 Correlation

Low correlation between the parameters is very important in the parameter identification process. Usually for PID analysis a correlation factor of 0.9 or higher between the regressors will result in poor parameter estimation [1]. Unfortunately some high correlation factors were found on data for both DA42 flight test projects. In general, the high correlation corresponds to the pitch rate and the elevator regressors for the longitudinal maneuvers. On the lateral-directional data, in general the highest correlation was found between the roll rate and aileron regressors. This may introduce some error on the derivatives of regressors with high correlation. The correlation in the frequency domain was expected to be higher than in the time domain, since the input was mainly designed for a time domain analysis. The following table shows the highest correlation factor for each test in the time domain and frequency domain for the DA42TDI project.

Table 9 Highest Correlation factor on the DA42TDI data

Case	TAS (Knots)	AOA (deg)	Time Domain		Frequency Domain	
			LON max. cor	LON max. cor	LAT max. cor	LAT max. cor
1	100	5.12	0.96	0.92	0.88	0.91
2	99	4.89	0.83	0.93	0.89	0.98
3	107	4.25	0.95	0.95	0.87	0.95
4	103	4.00	0.71	0.88	0.74	0.86
5	108	3.19	0.81	0.87	0.83	0.89
6	118	1.93	0.83	0.88	0.76	0.94
7	130	1.57	0.89	0.93	0.71	0.94
8	139	0.84	0.86	0.93	0.74	0.88
9	152	0.17	0.91	0.93	0.79	0.88
10	168	0.00	0.89	0.94	0.82	0.94
11	161	-0.05	0.91	0.95	0.81	0.92

The following table shows the highest correlation factor for each test in the time domain and frequency domain for the DA42L360 project.

Table 10 Highest Correlation factor on the DA42L360 data

Case	TAS (knots)	AOA (deg)	Time Domain		Frequency Domain	
			LON max. cor	LON max. cor	LAT max. cor	LAT max. cor
1	85	8.891	0.88	0.96	0.81	0.99
2	91	7.198	0.88	0.97	0.80	0.99
3	93	6.129	0.92	0.93	0.75	0.99
4	95	6.011	0.90	0.94	0.85	0.99
5	97	5.693	0.92	0.95	0.86	1.00
6	103	4.525	0.90	0.93	0.87	1.00
7	109	3.589	0.92	0.95	0.90	1.00
8	114	2.929	0.91	0.92	0.91	1.00
9	119	2.455	0.89	0.91	----	----
10	124	1.671	0.93	0.94	0.89	0.99
11	129	1.561	0.91	0.93	0.91	0.99
12	130	1.429	0.92	0.94	---	----
13	139	1.067	0.92	0.94	0.91	0.99
14	141	0.669	0.92	0.93	0.91	0.99
15	154	0.546	0.92	0.97	0.94	0.99
16	145	0.499	0.91	0.95	0.91	0.98
17	151	0.429	---	---	0.91	0.99
18	147	0.365	0.94	0.98	0.92	0.99
19	162	-0.023	0.92	0.95	0.92	0.99

As it can be seen from the tables above the correlation on the DA42L360 project in general was higher than for the DA42TDI. The biggest difference can be seen on the correlation for the lateral directional regressors. The high correlation factor on the DA42L360 corresponds to the aileron and roll rate regressors. Due to the high correlation factors on the frequency domain on the DA42L360, the output error on frequency domain was not applied to that data. As mentioned above, the aileron input on the DA42L360 was different from the one used in the DA42TDI program. The following figure is an example of the aileron and roll rate time histories for both projects.

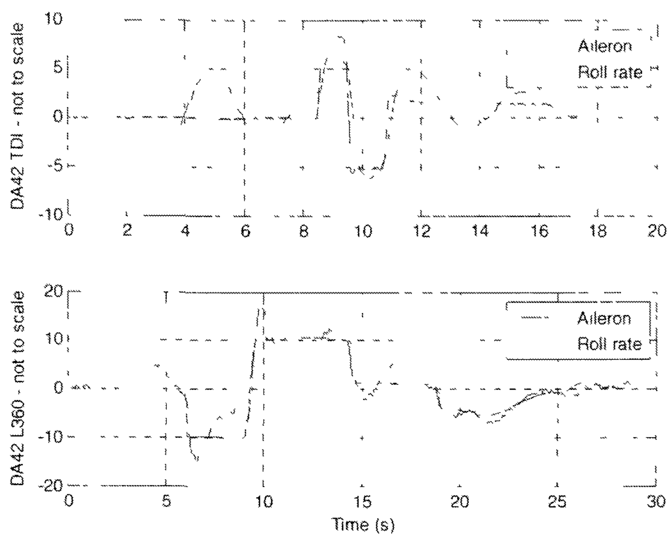

Figure 15 Aileron and roll rate time histories

2.9 Digital DATCOM analysis

The three view drawings provided by the AMM were input into CATIA and scaled 1:1 to measure the geometric characteristics of the DA42. Some important remarks about the digital DATCOM analysis are:

- Only 20 section cuts can be used to describe the fuselage
- Propeller power effects only apply to longitudinal stability
- Digital DATCOM only supports one ventral fin
- There is no function to model a rudder
- Digital DATCOM does not handles multiple bodies and there is no function to model the nacelles
- Wingtips do not affect longitudinal parameters

The following section shows in detail the information used to create the DATCOM input file. The three view drawings, the direct measurements on the airplane and the airplane specifications were used to create the model.

2.10 Flight Conditions (FLTCON)

In this section the flight conditions are defined. The following table shows all the flight condition at which the digital DATCOM model was run. The flight conditions were chosen to match the flight test points flown on the DA42TDI project.

Table 11 Digital DATCOM input file flight conditions

Case	Mach	Alpha (deg)	Altitude (ft)	Weight (lb)
1	0.151	5.12	5664	3741
2	0.149	4.89	5717	3753
3	0.161	4.25	5675	3759
4	0.155	4.00	5679	3686
5	0.163	3.19	5690	3692 •
6	0.178	1.93	5679	3701
7	0.196	1.57	5664	3712
8	0.210	0.84	5635	3723
9	0.229	0.17	5617	3734
10	0.254	0.00	5597	3764
11	0.243	-0.05	5603	3749

2.11 Reference Parameters (OPTINS)

This section was used to define the reference area and lengths. These are the same reference values used in the flight test programs.

Table 12 Digital DATCOM input file reference parameters

Name	Value	Units	Description	Source
ROUGFC[3]	0.00025	in	Surface roughness factor	For smooth paint[4]
SREF	175.300	ft^2	Reference area	AFM
CBARR	4.167	ft	Longitudinal reference length	AFM
BLREF	44.000	ft	Lateral reference length	AFM

2.12 Synthesis Parameters (SYNTHS)

In this section the basic configuration synthesis parameter are defined.

Table 13 Digital DATCOM input file Synthesis Parameters

Name	Value	Units	Description	Source
XCG	9.57	ft	Longitudinal location of C.G	Reference location
ZCG	-0.63	ft	Vertical Location of C.G	Approximated
XW	8.765	ft	Longitudinal location of theoretical wing	Measured (fig 1)
ZW	-1.25	ft	Vertical location of theoretical wing	Approximated
ALIW	3.00	deg	Wing root chord incidence angle	AMM
XH	24.660	ft	Longitudinal location on horizontal tail	Measured (fig 1)
ZH	3.905	ft	Vertical location on horizontal tail	Measured (fig 2)
ALIH	-1.00	deg	Horizontal tail root chord incidence angle	AMM
XV	23.086	ft	Longitudinal location on vertical tail	Measured (fig 2)
XVF	17.027	ft	Longitudinal location on Ventral Fin	Measured (fig 2)
ZV	0.000	ft	Vertical location on vertical tail	Measured (fig 2)
ZVF	0.345	ft	Vertical location on Ventral Fin	Measured (fig 2)

The following figure shows the reference drawings used in this section.

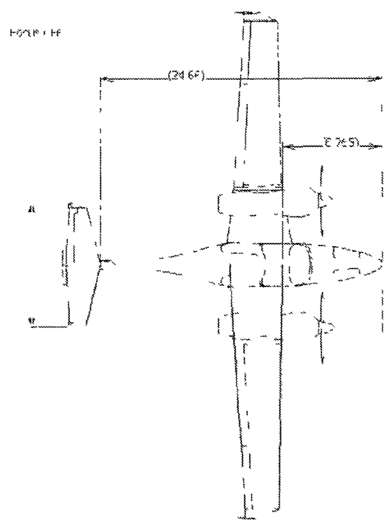

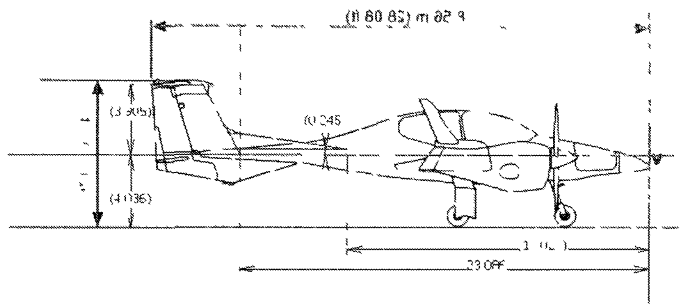

Figure 16 Reference drawings for Synthesis Parameters

2.13 Body Geometric Data (BODY)

In this section the body (fuselage) is described by using data coordinates. Twenty sections were split to define the body (maximum number allow by digital DATCOM). The spacing of the cuts is not constant with the intention of having more cuts where the slope changes were higher. The following drawing represents the 20 sections used.

Figure 17 Digital DATCOM body model

2.14 Wing Planform (WGPLNF)

In this section the geometry of the wing is described. The wing was approximated using the outer section of the DA42 wing.

Table 14 Digital DATCOM input file Wing Planform parameters

Name	Value	Units	Description	Source
CHRDTP	2.916	ft	Tip chord	Measured (fig 1)
SSPNE	20.145	ft	Semi-span exposed	Measured (fig 1)
SSPN	22.015	ft	Semi-span from theoretical root chord	Measured (fig 1)
CHRDR	4.632	ft	Root chord	Measured (fig 1)
SAVSI	1	deg	Sweep angle	AFM
CHSTAT	0.0	--	Reference chord for sweep angle, fraction of chord	AFM
TWISTA	0	deg	Twist angle	Assumed
DHDAO	5.5	deg	Semi-span dihedral	AMM
TYPE	1	--	Straight tapered planform	--

The following figure shows the reference drawings used in this section.

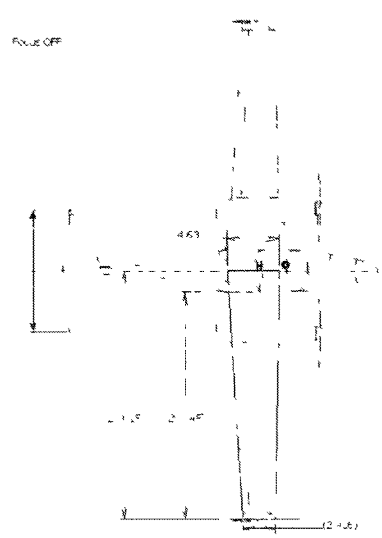

Figure 18 Reference drawing for wing planform parameters

2.15 Wing Airfoil (WGSCHR)

The airfoil shape was approximated by taking measurements on the DA42 wing and the airfoil information provided by the AFM. The DA42 airfoil is a Wortmann FX63-137/20-W4. The following figure shows the airfoil used on the digital DATCOM model.

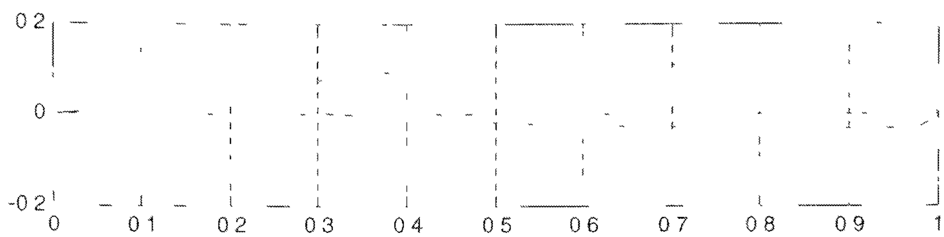

Figure 19 Wing airfoil model

2.16 Horizontal Tail Planform (HTPLNF)

In this section the geometry of the horizontal tail is described.

Table 15 Digital DATCOM input file horizontal tail planform parameters

Name	Value	Units	Description	Source
CHRDTP	1.414	ft	Tip chord	Measured (fig 1)
SSPNE	5.395	ft	Semi-span exposed	Measured (fig 1)
SSPN	5.395	ft	Semi-span from theoretical root chord	Measured (fig 1)
CHRDR	3.072	ft	Root chord	Measured (fig 1)
SAVSI	13.5	deg	Sweep angle	Measured (fig 1)
CHSTAT	0.25	--	Reference chord for sweep angle, fraction of chord	--
TWISTA	0	deg	Twist angle	Assumed
TYPE	1	--	Straight tapered planform	--

The following figure shows the reference drawings used in this section.

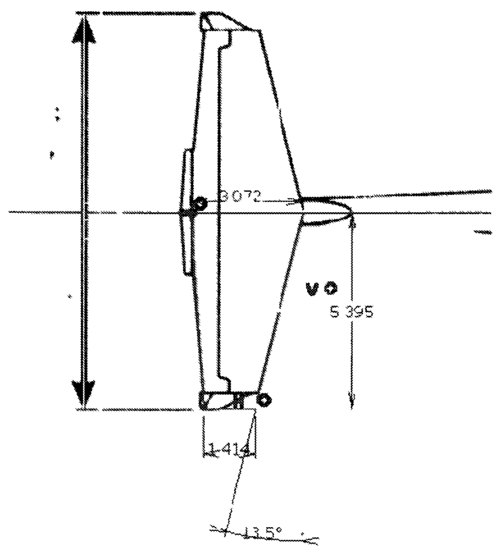

Figure 20 Reference drawing for horizontal tail parameters

2.17 Horizontal Tail Airfoil (HTSCHR)

The airfoil shape was approximated by taking measurements on the DA42 horizontal tail. The following figure shows the airfoil used on the digital DATCOM model.

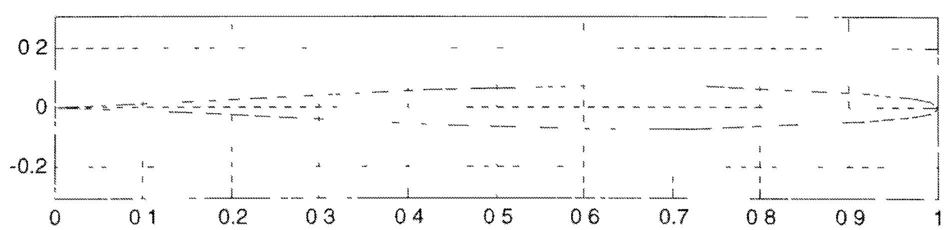

Figure 21 Horizontal tail airfoil model

2.18 Vertical Tail Planform (VTPLNF)

In this section the geometry of the vertical tail is described.

Table 16 Digital DATCOM input file Vertical Tail Planform parameters

Name	Value	Units	Description	Source
CHRDTP	2.857	ft	Tip chord	Measured (fig 1)
SSPNE	3.544	ft	Semi-span exposed	Measured (fig 1)
SSPN	3.905	ft	Semi-span from theoretical root chord	Measured (fig 1)
CHRDR	4.703	ft	Root chord	Measured (fig 1)
SAVSI	28.6	deg	Sweep angle	Measured (fig 1)
CHSTAT	0.25	--	Reference chord for sweep angle, fraction of chord	--
TYPE	1	--	Straight tapered planform	--

The following figure shows the reference drawings used in this section.

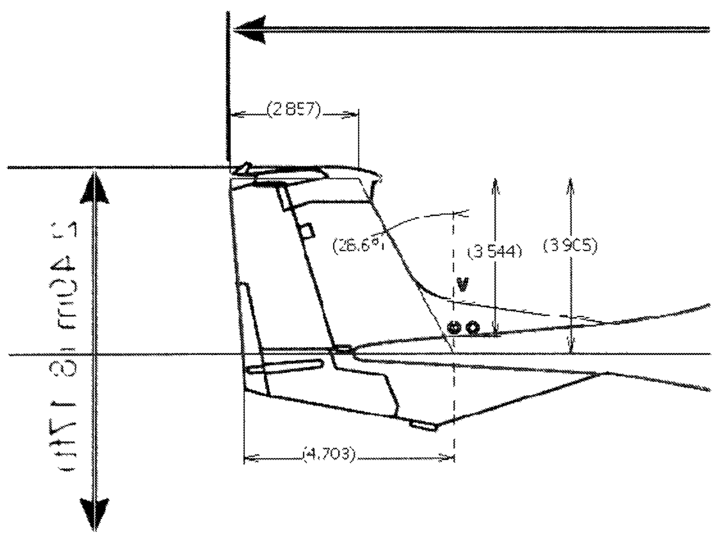

Figure 22 Reference drawing for vertical tail parameters

2.19 Vertical Tail Airfoil (VTSCHR)

The airfoil shape was approximated by taking measurements on the DA42 horizontal tail.

The following figure shows the airfoil used in the digital DATCOM model.

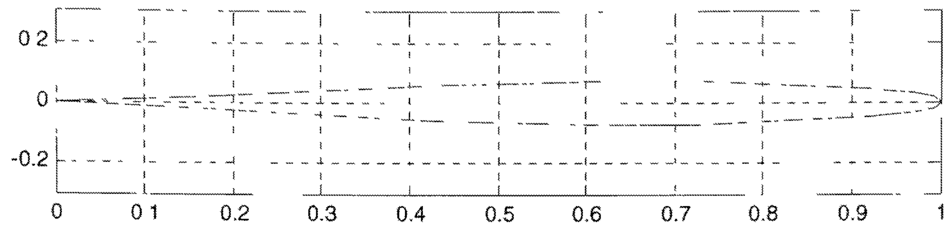

Figure 23 Vertical tail airfoil model

2.20 Ventral Fin (VFPLNF)

A ventral fin was added to model the top fin. The bottom fin was not added to this model because the ventral fin on digital DATCOM has to be above the reference line if the vertical tail is above the reference line. The following table and figure show the parameters used to model the ventral fin.

Table 17 Digital DATCOM input file Ventral Fin parameters

Name	Value	Units	Description	Source
CHRDTP	0.511	ft	Tip chord	Measured (fig 1)
SSPNE	0.507	ft	Semi-span exposed	Measured (fig 1)
SSPN	0.841	ft	Semi-span from theoretical root chord	Measured (fig 1)
CHRDR	6.256	ft	Root chord	Measured (fig 1)
SAVSI	82.265	deg	Sweep angle	Measured (fig 1)
CHSTAT	0.25	--	Reference chord for sweep angle, fraction of chord	--
TYPE	1	--	Straight tapered planform	--

The following figure shows the reference drawings used in this section.

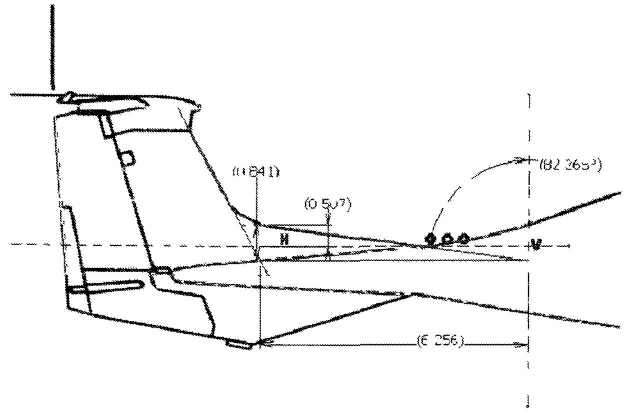

Figure 24 Reference drawing for Ventral Fin parameters

2.21 Wingtips - Twin vertical panels (TVTPAN)

The wing tips were approximated as vertical panels on the wigs. The following table shows the parameters used to model the wing tips.

Table 18 Digital DATCOM input file Wingtips parameters

Name	Value	Units	Description	Source
BVP	2.444	ft	Vertical Panel Span Above Lifting Surface	Measured (fig 1)
BV	2.444	ft	Vertical Panel Span	Measured (fig 1)
BDV	3.802	ft	Fuselage depth at quarter chord-point of vertical panel mean aerodynamic chord	Calculated form body coordinates
BH	44.03	ft	Distance between vertical panels	Measured (fig 1)
SV	2.10	ft^2	Planform area of one vertical panel	Estimated (fig 1)
VPHITE	10.00	deg	Total trailing edge angle of vertical panel airfoil section	Appr. From measurements on the DA42 wingtip
VLP	2.146	ft	Distance parallel to long. Axis between the c.g. and the quarter chord point of the MAC of the panel, positive if aft of c.g.	Measured (fig 1)
ZP	2.395	ft	Distance in the z-direction between the c.g. and the MAC of the panel, positive above c.g.	Measured (fig 1)

The following figure shows the reference drawings used in this section.

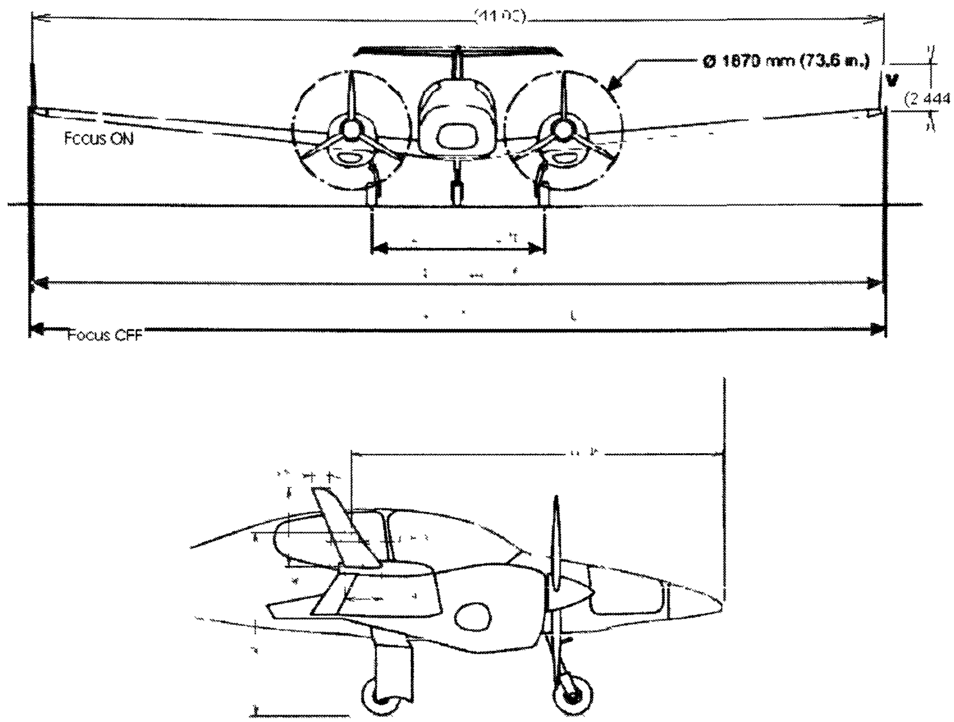

Figure 25 Reference drawings for Wingtip parameters

2.22 Propeller Power Parameters

The following table shows the parameters used to for the power model in digital DATCOM.

Table 19 Digital DATCOM input file Propeller Power parameters

Name	Value	Units	Description	Source
AIETLP	0.0	deg	Angle of incidence of engine thrust	Approx. (fig 1)
NENGSP	2.0	--	Number of engines	--
THSTCP	See Table 20	--	Thrust coefficient	FT data
PHALOC	5.253	ft	Axial location of propeller hub	Measured (fig 1)
PHAVLOC	0.135	ft	Vertical location of propeller hub	Measured (fig 1)
PRPRAD	3.067	ft	Propeller radius	AMM
ENGFCT	See Table 20		Normal force factor	Approximated using Reference 4
NOPBPE	3	--	Number of propeller blades per engine	--
BAPR75	See Table 20		Blade angle	FT data
YP	5.538		Lateral location of engine	Measured (fig 2)

Some of the power parameters depended on the flight condition. The power conditions were chosen to match the flight test points flown on the DA42TDI project. The following table shows the specific parameters used for each case.

Table 20 Power parameters for each flight condition

Case	AoA (deg)	THSTCP	BAPR75	ENGFCT
1	5.16	0.0628	22.12	1.29
2	5.2	0.0703	22.20	1.32
3	4.32	0.0584	22.59	1.29
4	3.89	0.0632	22.58	1.29
5	3.13	0.0543	22.88	1.26
6	2.01	0.0434	24.37	1.23
7	1.53	0.0381	26.00	1.18
8	0.82	0.0372	27.29	1.18
9	0.21	0.0328	28.01	1.16
10	-0.05	0.0348	27.69	1.16
11	-0.12	0.0333	28.26	1.16

The following figure shows the reference drawings used in this section.

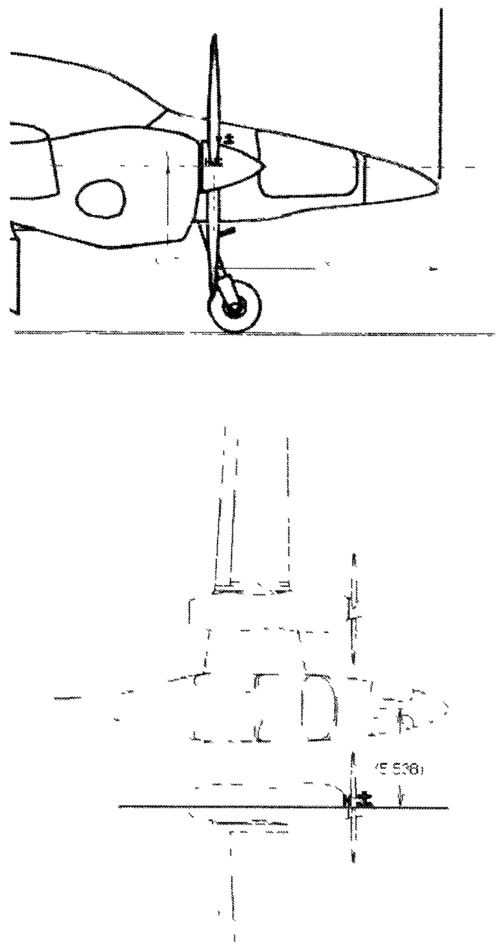

Figure 26 Reference drawing for Propeller Power parameters

2.23 Elevator – Symmetrical Flaps (SYMFLP)

The flaps or control surfaces in DATCOM are assumed to be located on the most aft lifting surface, in this case the horizontal tail. The following table shows the parameters used to model the elevator. The elevator was modeled as a plain flap on the horizontal tail.

Table 21 Digital DATCOM input file elevator parameters

Name	Value	Units	Description	Source
FTYPE	1	--	Plain Flap	--
NDELTA	9	--	Number of deflection angles	--
DELTA	-15 ,-10,-5,-2,0,2,5,10,13	deg	Deflection angle	--
PHETE	0.1135	--	Tangent of airfoil trailing edge based on 90 and 99 percent chord	Calculated from horizontal tail airfoil
PHETEP	0.0504	--	Tangent of airfoil trailing edge based on 95 and 99 percent chord	Calculated from horizontal tail airfoil
CHRDFI	1.057	ft	Elevator cord at inboard end of elevator	Approx. (fig 1-2)
CHRDFO	0.5881	ft	Elevator cord at outboard end of elevator	Approx. (fig 1-2)
SPANFI	0.0	ft	Span location of inboard end of elevator	Measured (fig 1)
SPANFO	4.928	ft	Span location of outboard end of elevator	Measured (fig 1)
CB	0.220	ft	Average chord of the balance	Approx. (fig 1-2)
TC	0.0737	ft	Average thickness of the control at hinge line	Approx. from horizontal tail airfoil
NTYPE	1	--		--

The following figure shows the reference drawings used in this section.

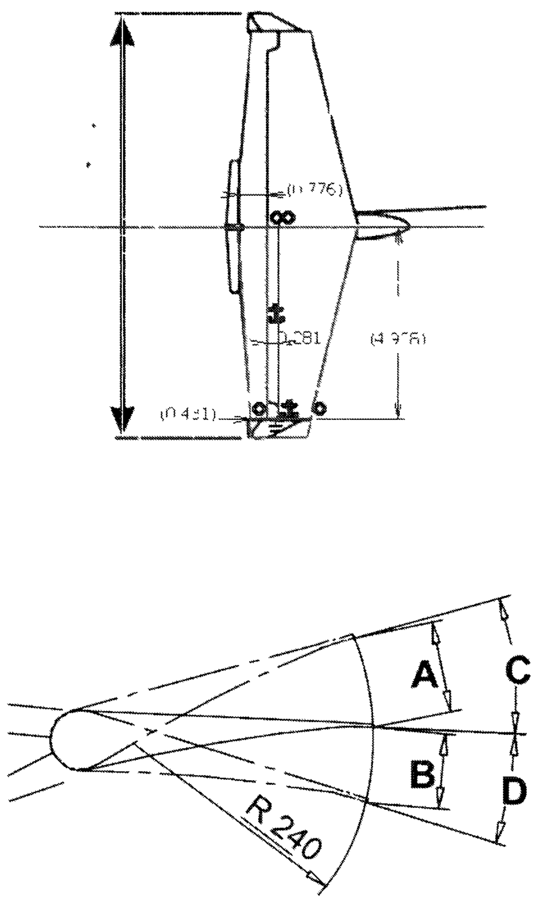

Figure 27 Reference drawings for Elevator parameters

2.24 MATLAB model

The following figure compares the three view drawings from the DA42 AMM with the model used for digital DATCOM. Unfortunately, the routine used to create the 3D view of the digital DATCOM model does not supports the ventral fin and vertical panels on the wings (wingtips).

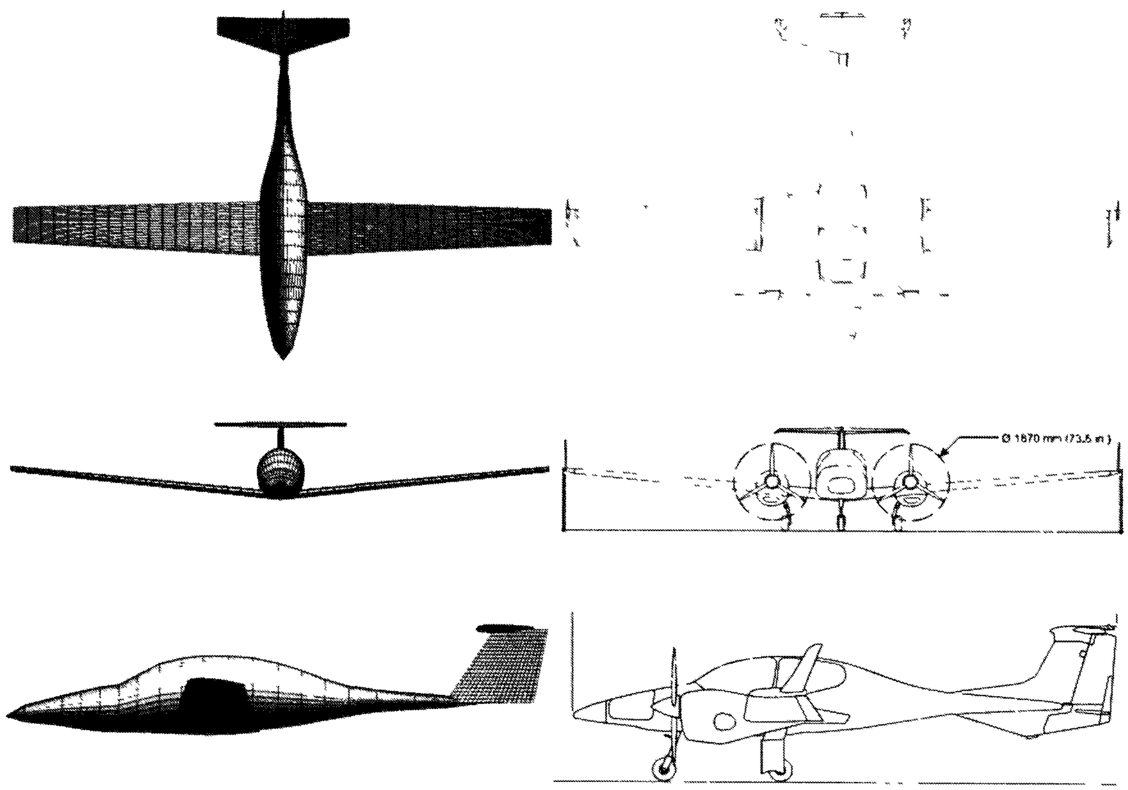

Figure 28 Three view model comparison

3. ANALYSIS AND RESULTS

3.1 Longitudinal

The lift force and pitching moment coefficient derivatives were estimated using the longitudinal maneuvers. The following sections show the results for the longitudinal mode from the PID analysis and the Digital DATCOM.

3.1.1 Lift force

The linear model used on the PID analysis for the lift force coefficient was:

$$CL = CL_{\alpha}a + CL_0$$

3.1.1.1 CL_{α}

The following values were estimated for CL_{α}.

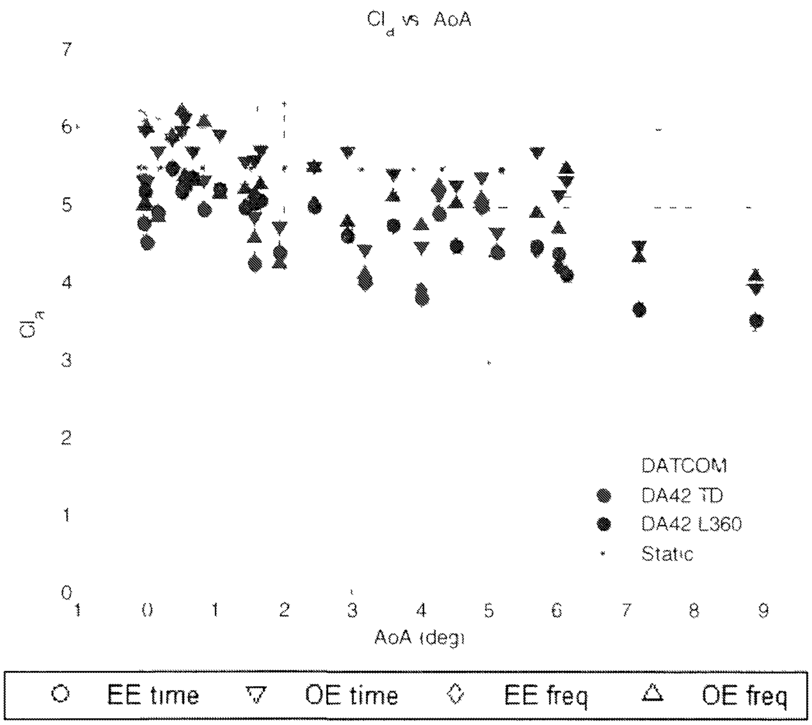

Figure 29 CL_{α} Results

The CL_{α} value obtained by the digital DATCOM analysis seems to be high considering the aspect ratio for the DA42. If the slope of a theoretical airfoil (2*pi) is corrected for the DA42 aspect ratio (11.06) the value for CL_{α} will be around 5.3 rad/s.

The CL_{α} "static" data shown in Figure 29 corresponds to the slope of the weight vs. alpha plot for the DA42TDI data during steady state flight.

3.1.2 Pitching Moment

The linear model used on the PID analysis for the pitching moment coefficient was:

$$Cm = Cm_{\alpha}a + Cm_{\hat{q}}\hat{q} + Cm_{\delta_e}\delta e + Cm_0$$

3.1.2.1 Cm_{α}

The following values were estimated for Cm_{α}.

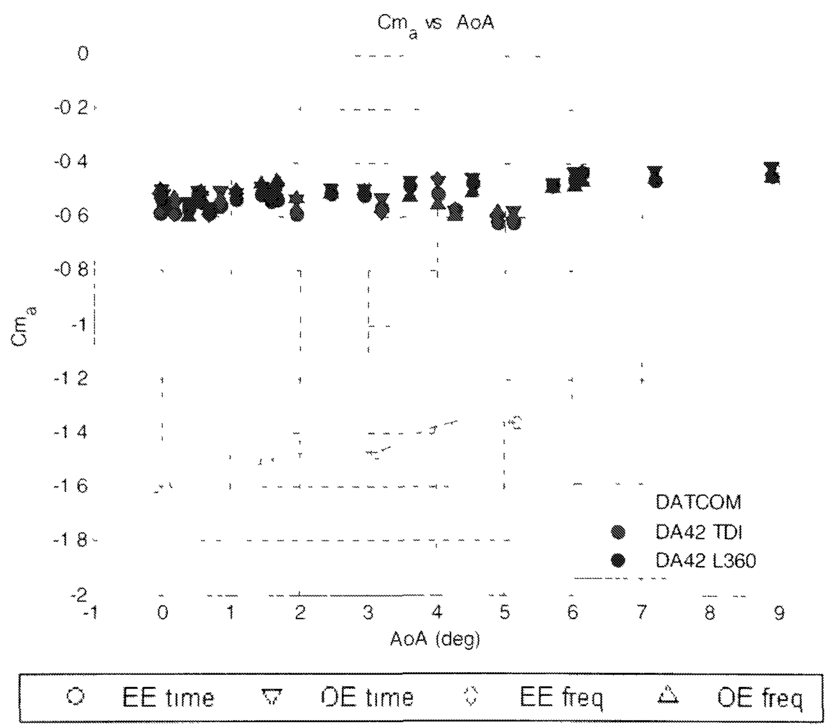

Figure 30 Cm_{α} results

The Cm_{α} results indicate an error on some of the measurements or on the reference parameters. Cm_{α} is a strong function of the longitudinal center of gravity (c.g); this suggests the main error may be on the c.g. measurements. However, there may be other parameters contributing to the discrepancy between digital DATCOM and the PID results for Cm_{α}. The vertical center of gravity was unknown in the flight test data and approximated on the digital DATCOM model. Other possible errors could be the estimation of the moment of inertia used to estimate the pitching moment coefficient.

To quantify the error between the PID and the digital DATCOM results for Cm_{α}, the static margin for each case was calculated. The following figure shows the results.

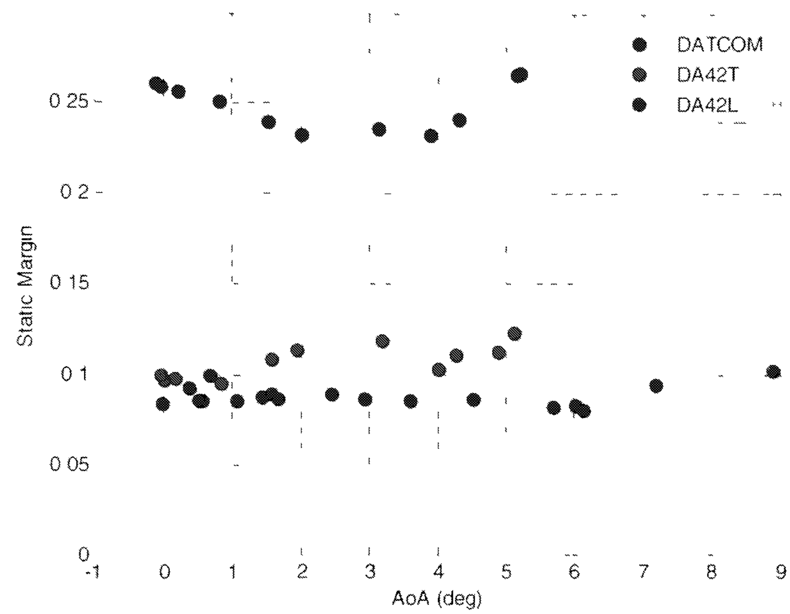

Figure 31 Static Margin Results

From Figure 31 it can be observed that the approximated error between the PID method and digital DATCOM is 15%, which corresponds to about 7.5in difference in the longitudinal c.g. This discrepancy may come from errors on the measurements and drawings used for the digital DATCOM model as well as errors on the estimation of the c.g. position on the flight test data.

3.1.2.2 Cm_q

The following values were estimated for Cm_q.

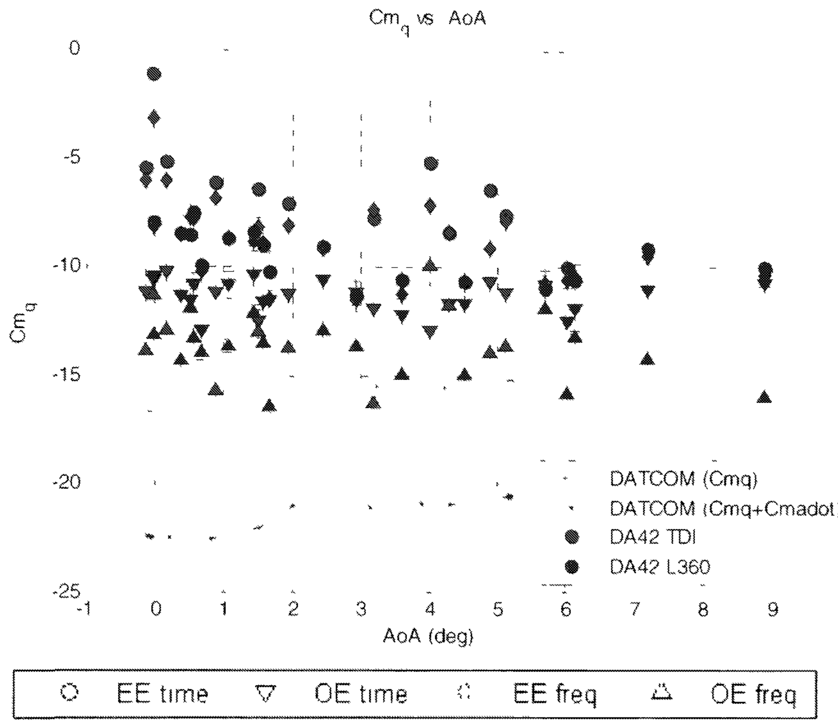

Figure 32 Cm_q Results

In parameter identification procedures the Cmq and $Cm_{\dot{\alpha}}$ derivatives are usually calculated as one damping derivative "Cmq". This is due to the high correlation between alphadot and pitch rate during PID maneuvers. As a consequence, the sum of the digital DATCOM results for Cm_q and $Cm_{\dot{\alpha}}$ was added to the plot. Significant scatter can be seen in Figure 32, especially on the Cm_q estimate for the DA42TDI. The scatter of the data may be explained by a combination of several factors. As it was mentioned before, a high correlation between the pitch rate and elevator was found in most of the data files. This is an indication of data collinearity between these two regressors, introducing possible errors on the estimates of Cm_q. Another factor could be a possible time delay in the INS data. The following figure shows an alpha reconstruction using INS data and the alpha measurement of the vane for the DA42TDI project.

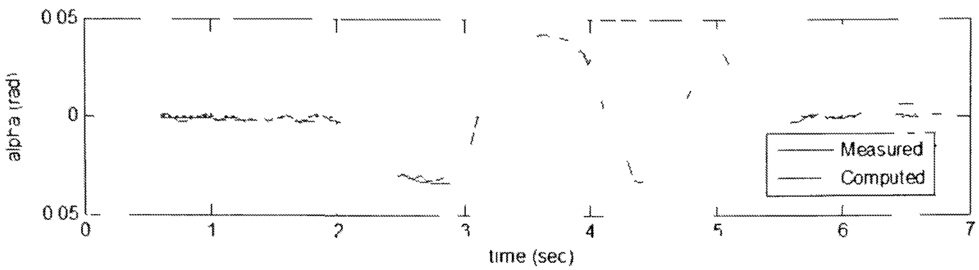

Figure 33 Alpha Reconstruction

Figure 33 shows a phase shift in the reconstruction of alpha This phase shift may be caused by errors on the alpha correction to the center of gravity which involves pitch rate This calculation was checked and the math was found to be correct, which indicates a possible lag on the INS data

3.1.2.3 $Cm_{\delta e}$

The following values were estimated for $Cm_{\delta e}$.

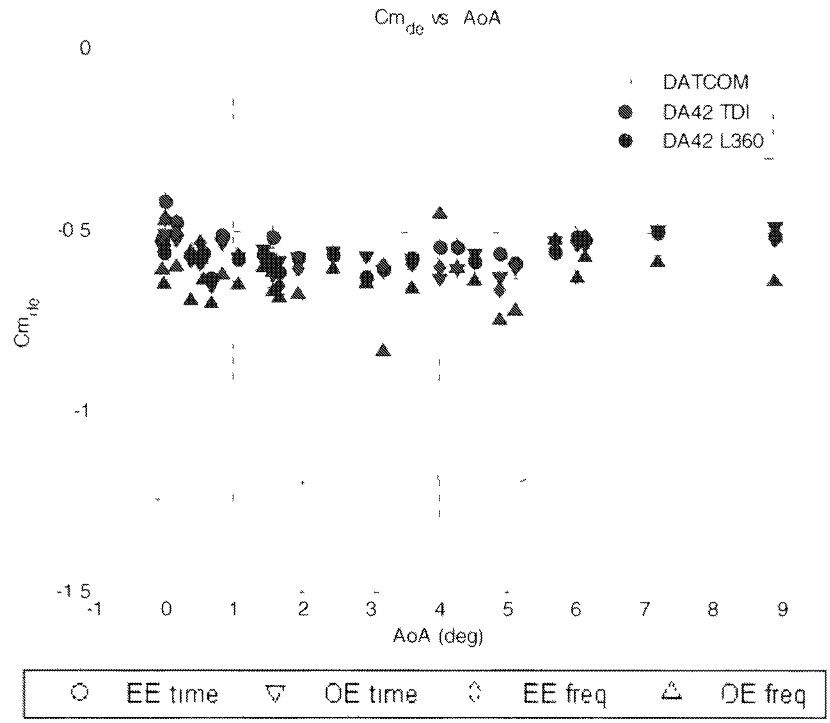

Figure 34 $Cm_{\delta e}$ Results

The results for $Cm_{\delta e}$ were consistent with the results for Cm_{α} in the sense that there seems to be an error on certain measurements like longitudinal center of gravity and/or moment of inertia.

3.2 Lateral - Directional

The side force, rolling moment and yawing moment coefficient derivatives were estimated using the lateral-directional maneuvers. The following sections show the results for the lateral-directional mode from the PID analysis and the Digital DATCOM.

3.2.1 Side Force

The linear model used on the PID analysis for the side force coefficient was:

$$CY = CY_{\beta}\beta + CY_{0}$$

3.2.1.1 CY_β

The following values were estimated for CY_β.

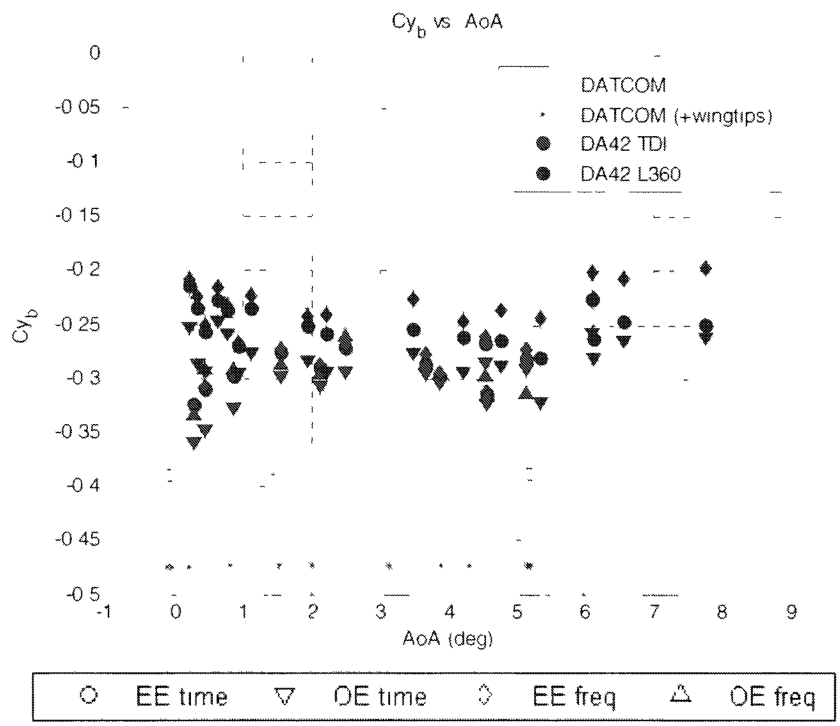

Figure 35 CY_β Results

As it can be seen on Figure 35, both the PID and the digital DATCOM results show no alpha dependency in the CY_β derivative. The CY_β estimate of digital DATCOM was about 25-30% higher than the one from the PID analysis. This discrepancy on the CY_β derivative may be caused by digital DATCOM treating the surface as a more flat-sided fuselage than the actual DA42 fuselage. In addition, it can be observable how the wingtips model increased the gap of the digital DATCOM and the PID methods estimated of CY_β. The results suggest that the wingtip model was misinterpreted by digital DATCOM. Also, it is important to remember that the bottom fin of the DA42 was not included on the digital DATCOM model.

3.2.2 Rolling Moment

The linear model used on the PID analysis for the rolling moment coefficient was:

$$Cl = Cl_{\beta}\beta + Cl_{\delta a}\delta a + Cl_{p}p + Cl_{r}r + Cl_{0}$$

3.2.2.1 Cl_{β}

The following values were estimated for Cl_{β}.

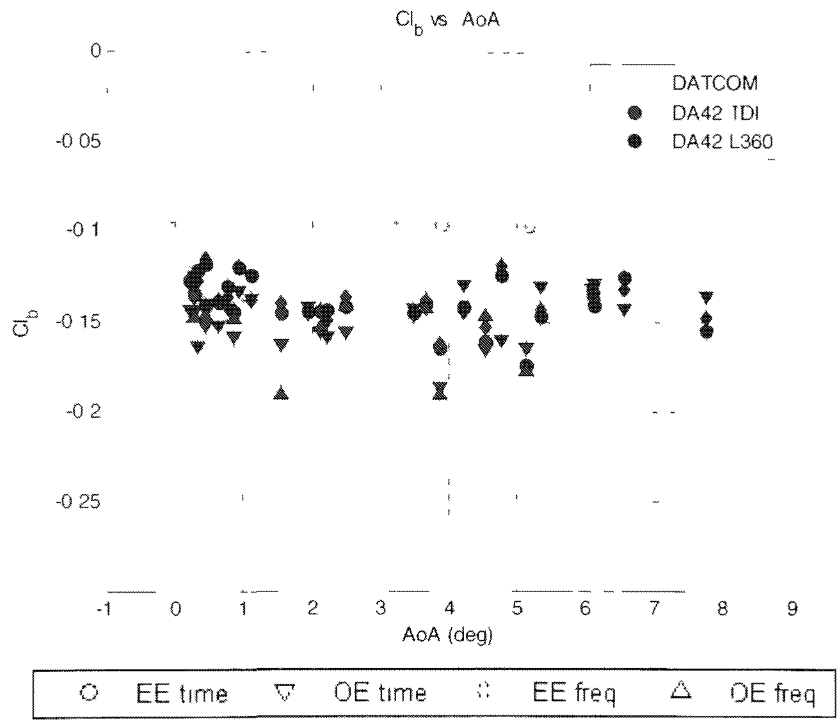

Figure 36 Cl_{β} Results

The estimation of Cl_{β} from the PID methods and digital DATCOM showed no dependency on angle of attack. From Figure 36, it can be seen that digital DATCOM underestimated the values for Cl_{β} compared to the PID results. The DA42 wings are made of carbon fiber and are very flexible which probably created higher dihedral angles in flight that digital DATCOM is not accounting for.

3.2.2.2 Cl_p

The following values were estimated for Cl_p.

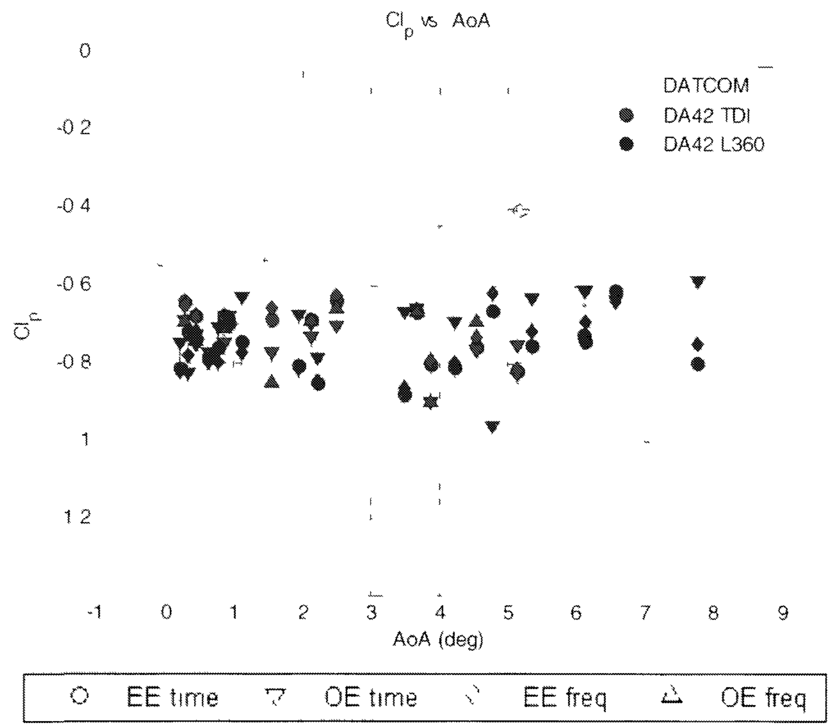

Figure 37 Cl_p Results

The data derivative results for both DA42s and digital DATCOM seem to have the same trend with alpha, however, the values from digital DATCOM were underestimated compared to the PID methods.

3.2.2.3 Cl_r

The following values were estimated for Cl_r

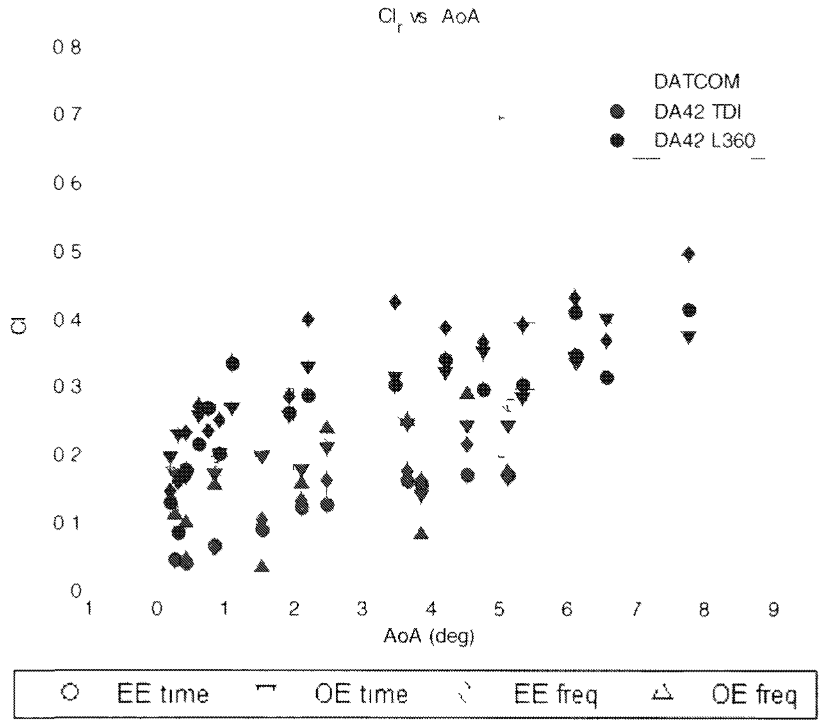

Figure 38 Cl_r Results

The digital DATCOM estimates of Cl_r laid within the PID results, following the same trend. An alpha dependency was found on the estimation of Cl_r. Usually the main contributors to the Cl_r derivative are the vertical tail and the wings. The wing contribution comes from an increase or decrease on dynamic pressure on one of the wings due to a yaw rate. This wing contribution to Cl_r probably introduces the alpha dependency observable on Figure 38.

3.2.2.4 $Cl_{\delta a}$

The following values were estimated for $Cl_{\delta a}$.

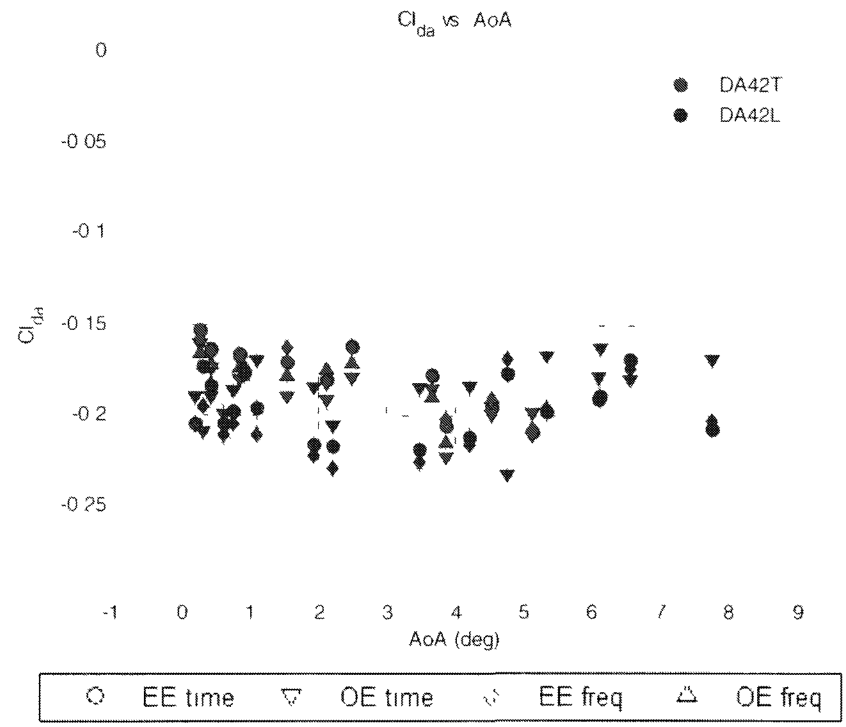

Figure 39 $Cl_{\delta a}$ Results

The $Cl_{\delta a}$ results for the DA42TDI and the DA42L360 were in agreement. This was expected since no modification was performed on the aileron control surfaces.

3.3 Yawing Moment

The linear model used on the PID analysis for the yawing moment coefficient was:

$$Cn = Cn_{\beta}\beta + Cn_{p}p + Cn_{r}r + Cn_{\delta r}\delta r + Cn_{0}$$

3.3.1.1 Cn_{β}

The following values were estimated for Cn_{β}.

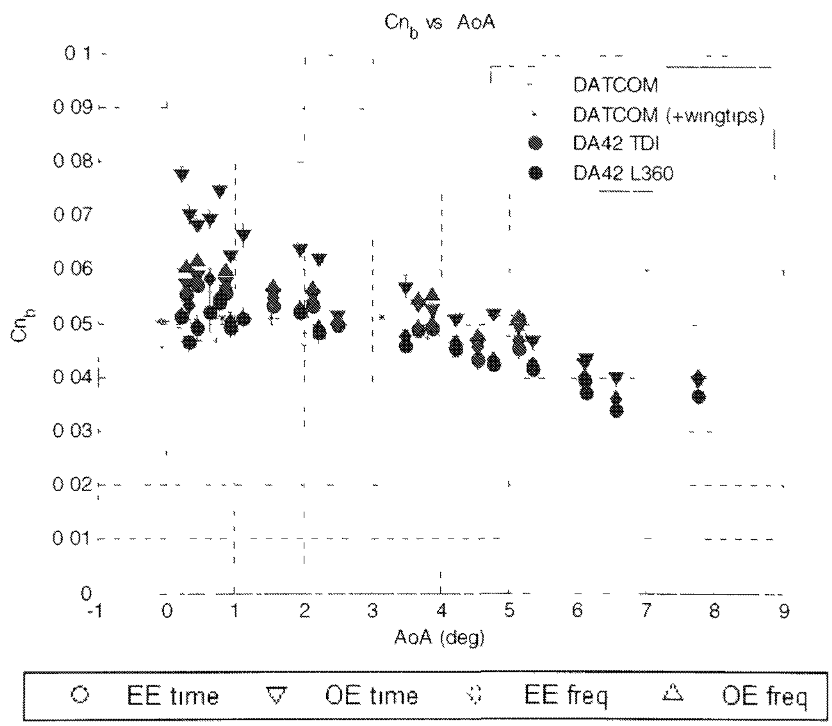

Figure 40 Cn_{β} Results

The main scatter on the data is due to the disagreement between the EE and OE methods estimation of Cn_{β} for the DA42 L360. The discrepancy between the two methods may be caused by the high correlation between the regressors on the DA42L360 data. As explained before, high correlation generally causes errors on the parameter estimation methods.

3.3.1.2 Cn_p

The following values were estimated for Cn_p.

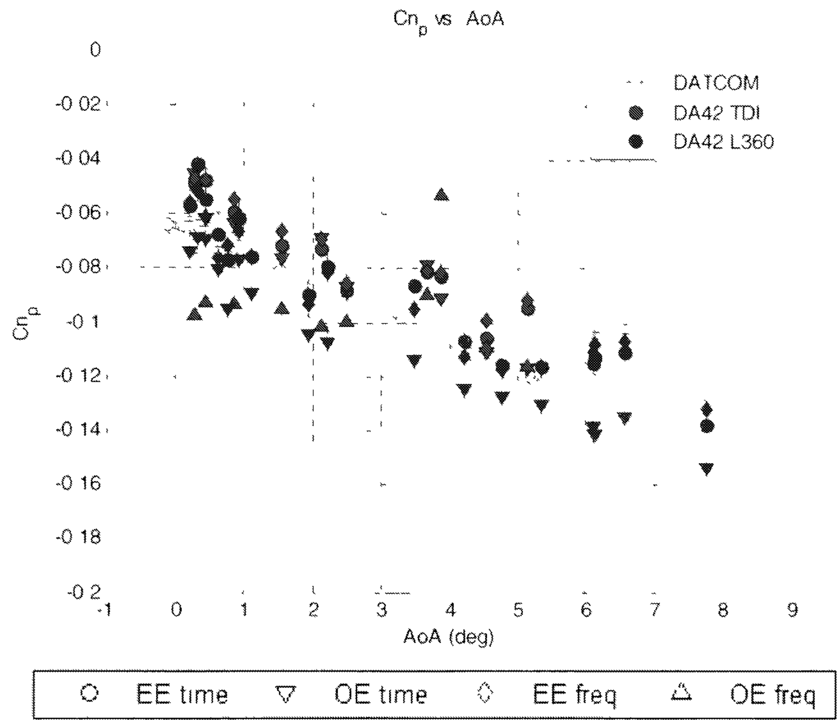

Figure 41 Cn_p Results

The results from the PID methods and digital DATCOM for Cn_p were consistent. All methods showed an alpha dependency on the estimation of Cn_p. Usually on the presence of a roll rate the wings will develop anti-symmetric drag. The main contributor is the induced drag on one wing due to differential angle of attack between the two wings caused by a roll rate.

3.3.1.3 Cn_r

The following values were estimated for Cn_r.

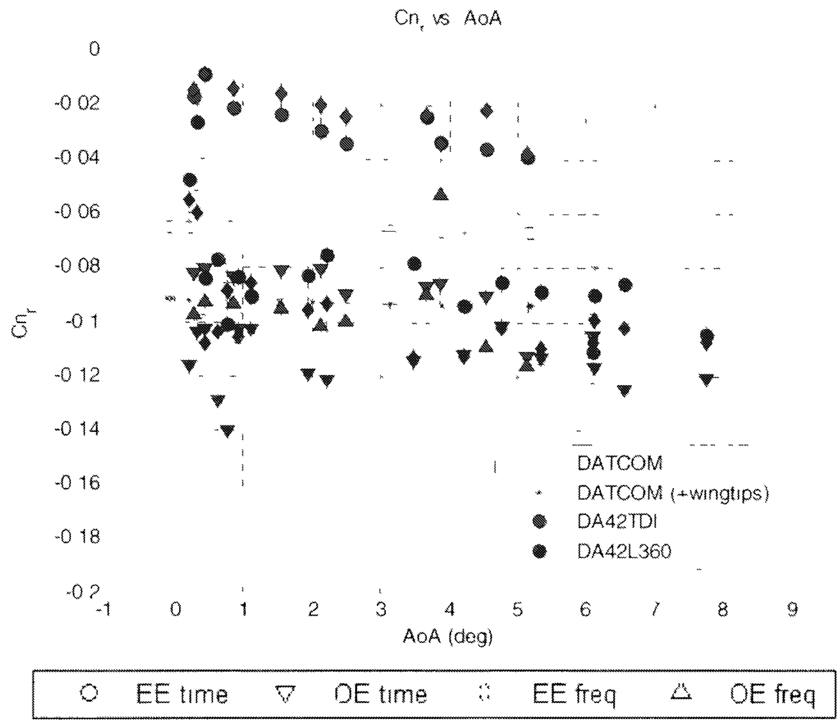

Figure 42 Cn_r Results

Figure 42 shows a wide scatter on the PID results for Cn_r. This scatter is consistent with other rotatory derivatives like Cm_q. As it was discussed for Cm_q it is possible that there was a lag on the DA42TDI INS data introducing errors on the estimation of Cn_r with the PID methods. In addition, as mentioned before, the results suggested that the wingtips model was interpreted incorrectly by digital DATCOM.

3.3.1.4 $Cn_{\delta r}$

The following values were estimated for $Cn_{\delta r}$.

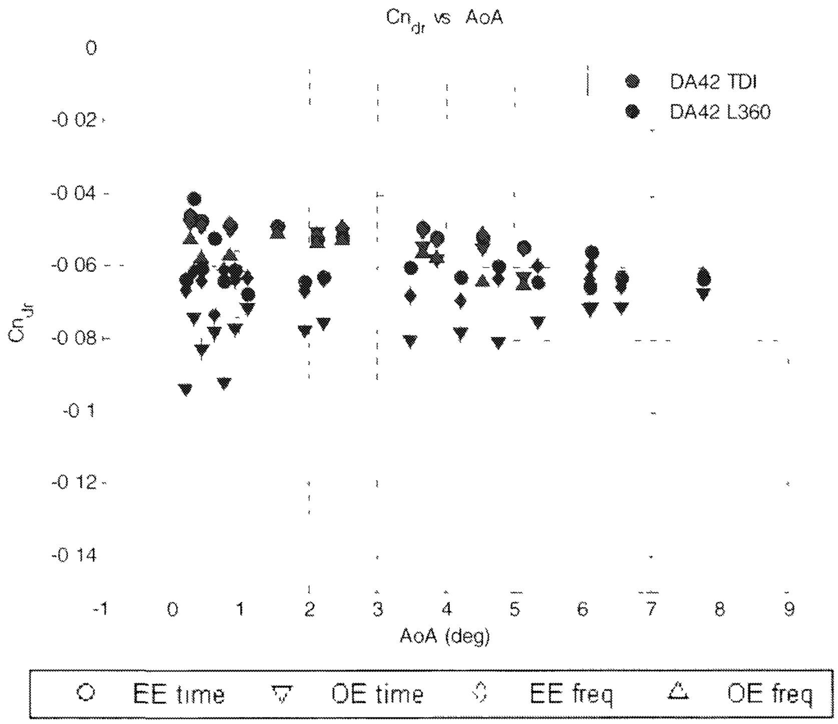

Figure 43 $Cn_{\delta r}$ Results

The main scatter in the data is due to the disagreement between EE and OE methods on the estimation of $Cn_{\delta r}$ for the DA42 L360. This coincides with the results for Cn_{β}. There are no results from digital DATCOM since this program does not support a rudder model.

4. CONCLUSION AND CORRELATION

4.1 Longitudinal Mode

The following table summarizes the estimated longitudinal derivatives from the PID analysis and digital DATCOM.

	CL_α	
	DA42 TDI	DA42 L360
EE time	$0.0771\alpha^2 - 0.4206\alpha + 4.8388$	$-0.1987\alpha + 5.3891$
OE time	$0.0888\alpha^2 - 0.5418\alpha + 5.4997$	$-0.0241\alpha^2 + 0.0205\alpha + 5.8401$
EE freq.	$0.075\alpha^2 - 0.4031\alpha + 4.8312$	$-0.2072\alpha + 5.4167$
OE freq.	$0.0901\alpha^2 - 0.5638\alpha + 5.461$	$-0.0117\alpha^2 - 0.035\alpha + 5.4657$
DATCOM	$-0.0143\alpha^3 + 0.0173\alpha^2 + 0.0841\alpha + 6.1609$	--

*Note: In the above equations α is in degrees

In general, it can be concluded that digital DATCOM overestimated CL_α compared with the results obtained from the PID analysis.

Table 22 Summary of Results for CL and Cm derivatives

	Cm_α		Cm_q		$Cm_{\delta e}$	
	DA42 TDI	DA42 L360	DA42 TDI	DA42 L360	DA42 TDI	DA42 L360
EE time	-0.57	-0.51	-6.04	-9.48	-0.53	-0.56
OE time	-0.54	-0.51	-11.36	-9.67	-0.58	-0.57
EE freq.	-0.57	-0.48	-7.09	-11.32	-0.56	-0.56
OE freq.	-0.55	-0.50	-13.26	-13.86	-0.63	- 0.63
DATCOM	-1.48	--	-15.84	--	-1.20	--

As it was discussed in the analysis section the biggest scatter in the longitudinal parameters was found on the Cm_q derivative. A possible explanation for this could be the high correlation between pitch rate and the elevator or the presence of lag in the INS data.

In general, there was a significant difference on the estimated value of the pitch coefficient derivatives by DATCOM and the PID methods. Better measurements of the airplane geometry and the center of gravity may improve the estimation of these derivatives.

4.2 Lateral-Directional Mode

The following tables summarize the estimated lateral-directional derivatives from the PID analysis and Digital DATCOM. The lateral-directional DA42L360 data could not be analyzed using the output error algorithm on the frequency domain due to the high correlation between the parameters.

Table 23 Summary of Results for CY derivatives

	CY_β	
	DA42 TDI	DA42 L360
EE time	-0.29	-0.25
OE time	-0.31	-0.28
EE freq.	-0.29	-0.23
OE freq.	-0.30	--
DATCOM	-0.39	--

The CY_β estimate of digital DATCOM was about 25-30% higher than the one from the PID analysis.

Table 24 Summary of Results for Cl derivatives

	Cl_{β}		Cl_{p}		Cl_{r}		$Cl_{\delta a}$	
	DA42 TDI	DA42 L360	DA42 TDI	DA42 L360	DA42 TDI	DA42 L360	DA42 TDI	DA42 L360
EE time	-0.15	-0.13	-0.70	-0.76	$-0.0049\alpha^2 + 0.0544\alpha + 0.0265$	$0.0029\alpha^3$ $0.0374\alpha^2 + 0.1575\alpha + 0.1141$	-0.18	-0.20
OE time	-0.16	-0.14	-0.74	-0.70	$0.0016\alpha^2 + 0.0047\alpha + 0.1735$	$-0.0022\alpha^2 + 0.0377\alpha + 0.21$	-0.19	-0.19
EE freq.	-0.15	-0.14	-0.70	-0.75	$-0.008\alpha^2 + 0.0737\alpha + 0.0175$	$0.0034\alpha^3$ $0.045\alpha^2 + 0.1936\alpha + 0.1302$	-0.18	-0.20
OE freq.	-0.16	--	-0.74	--	$0.0248\alpha + 0.1004$	--	-0.18	--
DATCOM	-0.09	--	-0.49	--	$0.0203\alpha + 0.1741$	--	--	--

*Note: In the above equations α is in degrees

The estimated Cl derivatives had the same trend between all the methods, however; in general digital DATCOM underestimated the derivative values compared to the PID results.

Table 25 Summary of Results for Cn derivatives

	Cn_β		Cn_p		Cn_r		$Cn_{\delta r}$	
	DA42 TDI	DA42 L360	DA42 TDI	DA42 L360	DA42 TDI	DA42 L360	DA42 TDI	DA42 L360
EE time	0.051	0.046	$0.0016\alpha^2 - 0.0182\alpha - 0.0436$	$0.0006\alpha^2 - 0.0145\alpha - 0.0535$	-0.027	-0.083	-0.050	0.060
OE time	0.054	0.058	$-0.011\alpha - 0.0489$	$0.0008\alpha^2 - 0.0161\alpha - 0.07$	-0.087	-0.114	-0.053	0.077
EE freq.	0.052	0.048	$0.0016\alpha^2 - 0.0182\alpha - 0.0411$	$0.001\alpha^2 - 0.0161\alpha - 0.0562$	-0.022	-0.097	-0.050	0.064
OE freq.	0.056	--	$-0.0118\alpha - 0.0505$	--	-0.095	--	-0.056	--
DATCOM	0.047	--	$-0.0105\alpha - 0.0653$	--	-0.066	--	--	--

*Note: In the above equations α is in degrees

The PID methods used on the estimation of Cn_β and $Cn_{\delta r}$ disagree at low angle of attacks. In general, the digital DATCOM results were within or relative close to the PID derivative estimates. In addition, the results suggest that the wingtip model was misinterpreted by digital DATCOM.

4.3 Future work

The data found on this research project raised new questions and opened the door for future research projects.

- Analyze high scale factors on alpha and beta on the data compatibility analysis and relate the associated error with the errors on the stability and control derivatives estimates. On this research high scale factors up to almost 25% percent were found. The scale factor on alpha and beta affects directly the stability derivative estimates

- Analyze the relationship between the correlation factors and the stability and control derivatives estimated by the parameter identification methods
- Analyze the power effect on the stability and control derivatives using theoretical verification methods
- CFD is beginning to play a very important roll on the design of airplanes. The results from this research could be compared to other analytical techniques such as CFD
- A wide scatter was found on the damping derivatives, some possible causes were suggested on this research. However, further analysis could reveal other possible causes and ways of improving the data to obtain better estimates of the stability and control derivatives
- Improve inputs for better parameter identification by reducing data collinearity. Also, there could be some input design before the next flight test program to optimize the content on the data and to excite the desired modes

5. REFERENCES

[1] Klein, Vladislav, and Eugene A. Morelli. Aircraft System Identification - Theory and Practice. Reston: American Institute and Aeronautics and Astronautics, Inc., 2006

[2] Jategaonkar, Ravindra V. Flight Vehicle System Identification - A Time Domain Methodology. Reston: American Institute and Aeronautics and Astronautics, Inc., 2006

[3] THE USAF STABILITY AND CONTROL DIGITAL DATCOM Volume I, Users Manual. St. Louis: Mcdonnell Douglas astronautics company – St. Louis division., 1980.

[4] Raymer, Daniel P. Aircraft Design: A Conceptual Approach Fourth Edition. Reston: American Institute and Aeronautics and Astronautics, Inc., 2006

6. APPENDIX 1: STEPWISE REGRESSION

To determine the most significant derivatives the stepwise regression function form SIDPAC was used. When running the stepwise regression function close attention was paid to the following criteria:

- R squared value (Should be as close to 100% as possible)
- F ratio (Should be above 20 for each derivative)
- PSE number (Should be as small as possible)

For the longitudinal mode the following regressors were used:

1- Alpha

2- qhat

3- Elevator

The following examples were run for the lift and pitching moment coefficients.

A1. Lift coefficient

STEP 1

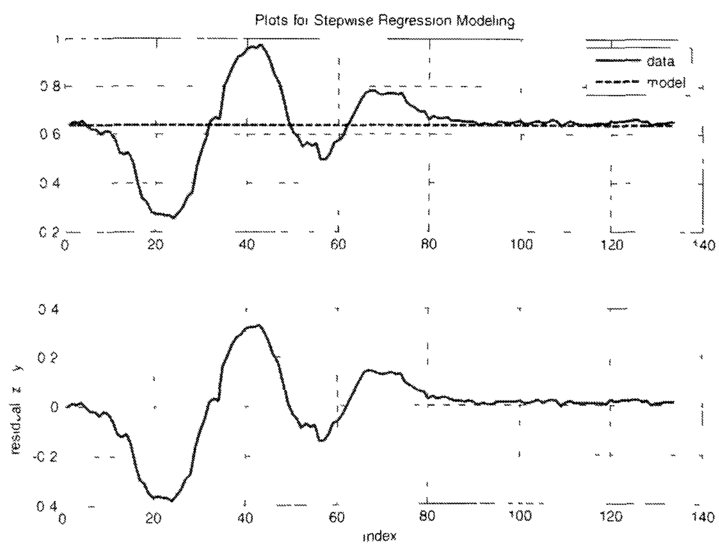

	Parameters		F ratio	Squared Part. Corr.
No.	Estimate	Change	In	Out
1	0.0000e+000	0.0000e+000	0.0000e+000	0.95424
2	0.0000e+000	0.0000e+000	0.0000e+000	0.19242
3	0.0000e+000	0.0000e+000	0.0000e+000	0.13801

constant term = 6.3864e-001   F cut-off value = 20.00

dependent variable rms value = 6.5516e-001

fit error = 1.467437e-001 or 22.40 percent

R squared = 0.00 %   PRESS = 2.9072e+000

PSE = 2.1534e-002

STEP 2

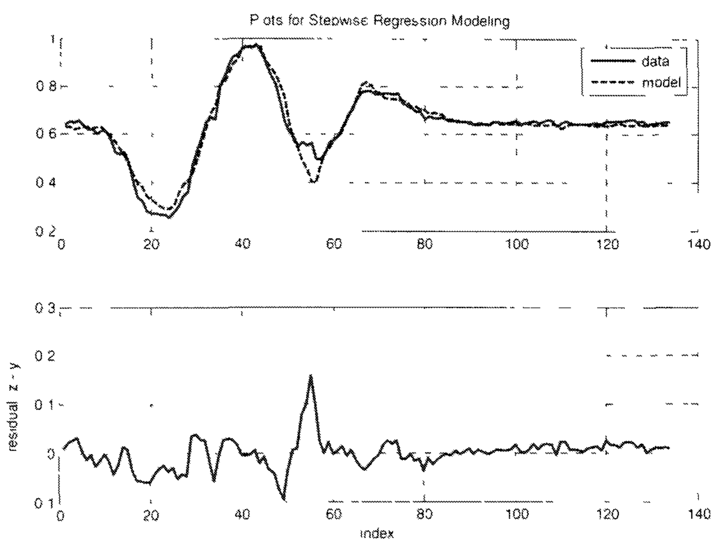

No.	Parameters Estimate	Change	F ratio In	Squared Part. Corr. Out
1	4.8178e+000	4.8178e+000	2.7529e+003	0.00000
2	0.0000e+000	0.0000e+000	0.0000e+000	0.02456
3	0.0000e+000	0.0000e+000	0.0000e+000	0.12455

constant term = 3.6488e-001 F cut-off value = 20.00

dependent variable rms value = 6.5516e-001

fit error = 3.150795e-002 or 4.81 percent

R squared = 95.42 % PRESS = 1.3726e-001
PSE = 1.2993e-003

STEP 3

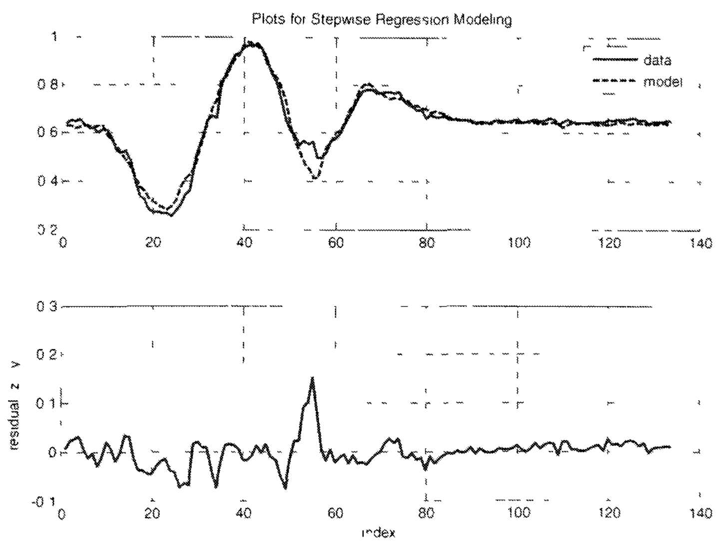

Parameters			F ratio	Squared Part. Corr.
No.	Estimate	Change	In	Out
1	4.6978e+000	-1.1999e-001	2.6880e+003	0.00000
2	0.0000e+000	0.0000e+000	0.0000e+000	0.13283
3	-2.7159e-001	-2.7159e-001	1.8637e+001	0.00000

constant term = 3.5724e-001 F cut-off value = 20.00

dependent variable rms value = 6.5516e-001

fit error = 2.959294e-002 or 4.52 percent

R squared = 95.99 % PRESS = 1.2292e-001
PSE = 1.3382e-003

NOTE

The elevator should not be included because:

- F ratio less than 20
- PSE increased
- regressors

A2. Pitching Moment coefficient

STEP 1

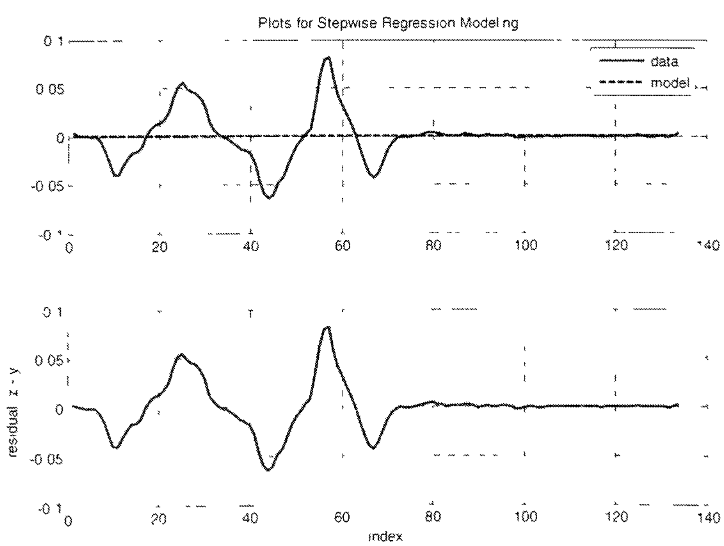

	Parameters		F ratio	Squared Part. Corr.
No.	Estimate	Change	In	Out
1	0.0000e+000	0.0000e+000	0.0000e+000	0.53131
2	0.0000e+000	0.0000e+000	0.0000e+000	0.00000
3	0.0000e+000	0.0000e+000	0.0000e+000	0.08788

constant term = 1.4390e-004   F cut-off value = 20.00

dependent variable rms value = 2.3840e-002

fit error = 2.392855e-002 or 100.37 percent

R squared = 0.00 %   PPESS = 7.7302e-002

PSE = 5.7258e-004

STEP 2

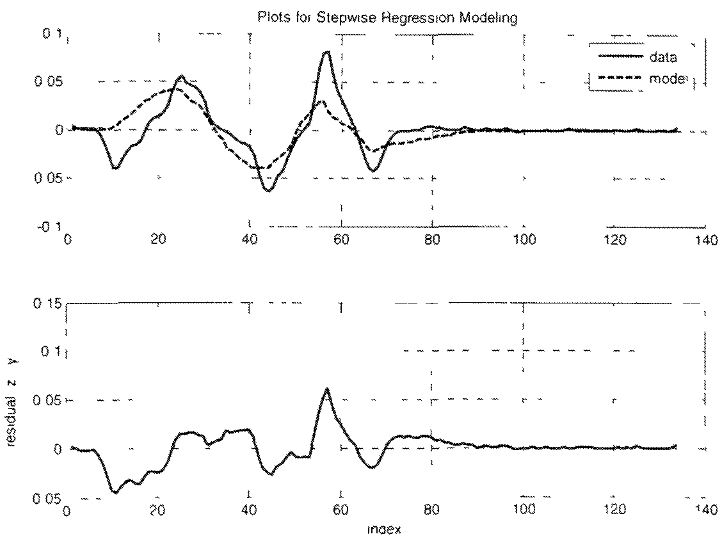

	Parameters		F ratio	Squared Part. Corr.
No.	Estimate	Change	In	Out
---	--------	------	--	---
1	-5.8621e-001	-5.8621e-001	1.4964e+002	0.00000
2	0.0000e+000	0.0000e+000	0.0000e+000	0.24168
3	0.0000e+000	0.0000e+000	0.0000e+000	0.63693

constant term = 3.3453e-002 F cut-off value = 20.00

dependent variable rms value = 2.3840e-002

fit error = 1.644364e-002 or 68.98 percent

R squared = 53.13 % PPRESS = 3.7194e-002

PSE = 2.7490e-004

STEP 3

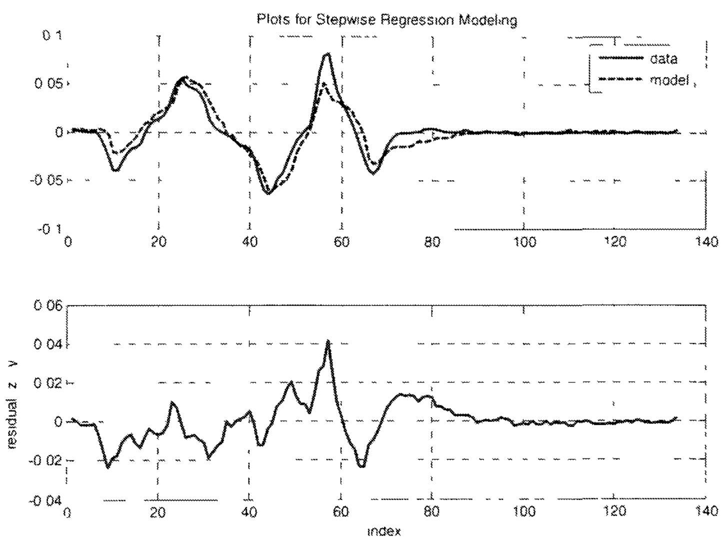

Parameters			F ratio	Squared Part. Corr.
No.	Estimate	Change	In	Out
1	-7.2782e-001	-1.4161e-001	5.7118e+002	0.00000
2	0.0000e+000	0.0000e+000	0.0000e+000	0.61508
3	-3.2054e-001	-3.2054e-001	2.2981e+002	0.00000

constant term = 2.4429e-002 F cut-off value = 20.00

dependent variable rms value = 2.3840e-002

fit error = 9.945933e-003 or 41.72 percent

R squared = 82.98 % PRESS = 1.3774e-002

PSE = 1.0953e-004

STEP 4

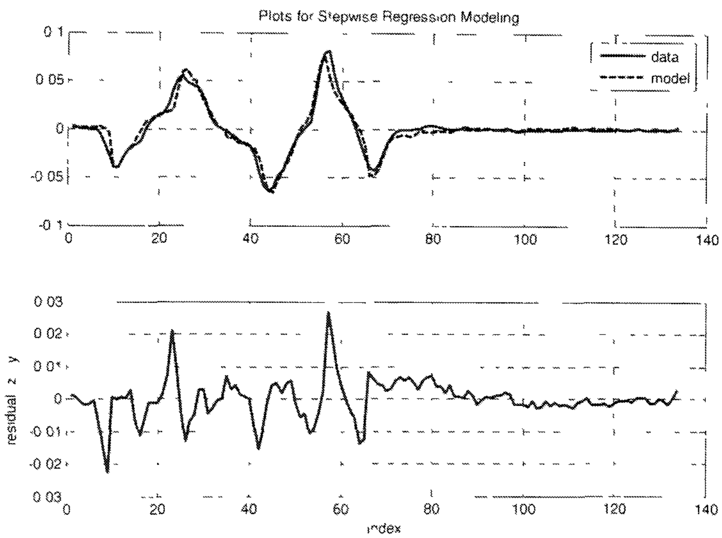

			Squared
Parameters		F ratio	Part. Corr.

No.	Estimate	Change	In	Out
1	-6.2947e-001	9.8356e-002	9.7520e+002	0.00000
2	-1.2736e+001	-1.2736e+001	2.0773e+002	0.00000
3	-6.8731e-001	-3.6678e-001	5.7539e+002	0.00000

constant term = -9.6994e-004 F cut-off value = 20.00

dependent variable rms value = 2.3840e-002

fit error = 6.194356e-003 or 25.98 percent

R squared = 93.45 % PRESS = 5.4545e-003
PSE = 5.4316e-005